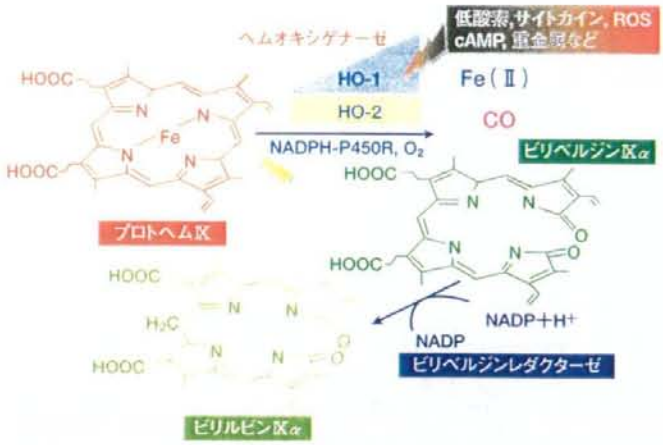

図3. HOによるCOの生成と誘導型酵素HO-1の誘導刺激

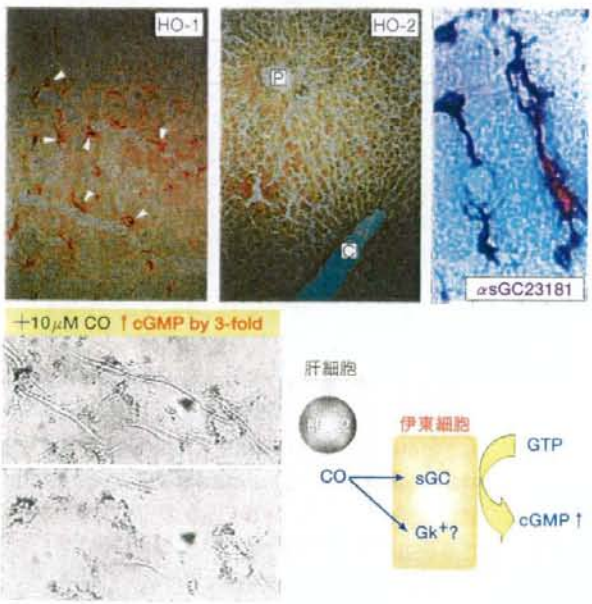

図4. 肝臓におけるHO-1, HO-2の発現（左上）とsGCの伊東細胞における発現（右上）

sGCの単クローン抗体MAb23187による染色性（褐色）は伊東細胞に局在．茶色はクッパー細胞．初代培養伊東細胞は細胞突起同士が牽引することでシリコン膜の"しわ"を形成するが，cGMPの上昇とともにCOの添加で"しわ"は消失し，細胞の弛緩を起こしたことが示される．C：中心細静脈，P：門脈終末枝．左上：Goda N, et al: J Clin Invest (1998) 101: 604-612より改変．

血管抵抗を低く維持するような特有の巧妙な仕組みが存在することになる．ラット肝臓を*ex vivo*で灌流すると，静脈灌流液中には数百μM程度のCOが検出される．外から灌流されたCOは拡散律速で肝臓全体に分布すること，肝臓の血流量と実質組織体積を勘案したモデリングから，Disse腔周辺のCO濃度はおそらく5～10μMに及ぶと考えられる．内因性COをHO阻害剤であるZincプロトポルフィリンⅨ(ZnPP)で消去，あるいはCO自身を捕捉するヘモグロビンを投与すると血管抵抗の著明な増加が起こった[2), 3)]．またCOを捕捉できないメトヘモグロビンの投与ではこのような変化が起こらなかった．さらに，遊離ヘモグロビンをfenestrationを通過できないようにリポソームで封入すると，血管抵抗増加作用は消失した．CO生成低下時の血管収縮は小葉内の類洞血管に起きており，肝臓特異的な血管周皮細胞である伊東細胞の局在に一致した．このことからCOの受容系は，伊東細胞に存在すると考えられた．初代培養した伊東細胞は，培養液に添加したμMレベルのCOにより可溶性グアニル酸シクラーゼ(sGC)が活性化されcGMPの増加を認め，この細胞は肝臓における主要なsGCのリソースであることも明らかになった（図4）．薄いシリコン膜上に伊東細胞を高密度で培養すると，細胞突起が連携することで膜に"しわ"が寄り，10μM程度のCOの表面灌流を行うと"しわ"の形成が解除されたことから，主に肝臓実質細胞のHO-2で生成されたCOが赤血球のヘモグロビンに到達する前に伊東細胞のsGCに作用し，恒常的に血管を弛緩させているものと考えた．

しかしながら，COによるsGCの活性化能はNOのそれに比べてはるかに小さいことは昔から良く知られていた．培養細胞や臓器レベルの実験結果からCOが細胞内あるいは臓器内のcGMPを増加させることが報告されている．しかしながらCOによる*in vitro*でのsGCの活性化能はNOのそれに比してきわめて低く，本酵素のV_{max}は十分量のガス分子が存在する場合，NOでは200倍程度に増加するのに対しCOでは2～3倍程度である[6)]．すなわちCOはNOと比べてsGCの弱い活性化物質でしかない．このような違いはガス分子がヘムに配位した際の構造変化の違いに起因しており，NOの場合は配位すると鉄原子が遠位側に偏位して酵素分子のβサブユニットにある近位ヒスチジンの配位結合が切れて5配位型になるのに対し，COの場合は配位後に上記のような鉄原子の偏位が起きないため6配位型を保つことが明らかになった．このようなガス分子の配位に伴う機能変化の違いのため，精製したsGCに*in vitro*でCOを加えるとNOのない系では活性化が起こるが，NOであらかじめ活性化させた酵素

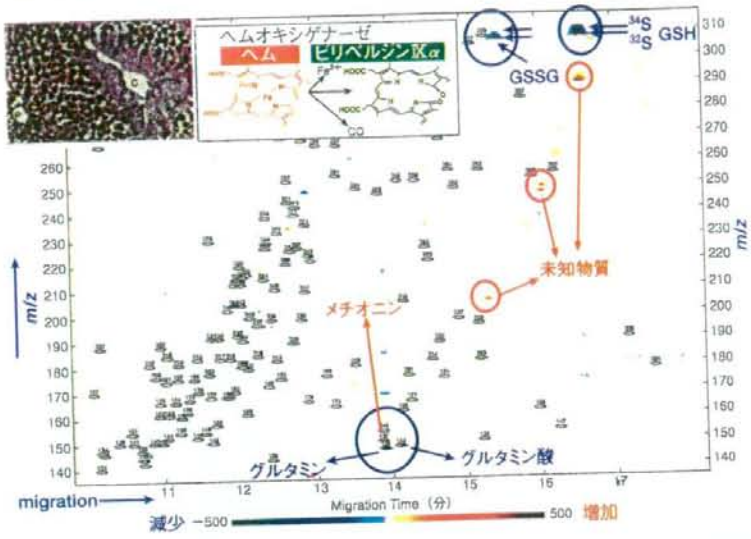

図5. マウスにおけるアセトアミノフェン肝障害モデルにおける小葉中心性壊死の形成とメタボローム解析

DMD (differential metabolomics display) の技術によって正常肝臓と薬剤投与後にCOの生成が最大になる条件で，増加する代謝物（赤）と減少する代謝物（青）を一括表示したものの一部分を示す．横軸は電気泳動時間，縦軸は質量数を電荷で割った値（m/z）を示す．○はKEGG (Kyoto Encyclopedia of Genes and Genomes) データベースに掲載されている既知化合物の出現部位を示している．既知物質ではメチオニンの増加，グルタミン酸，グルタミンの低下，酸化型・還元型グルタチオンの低下が確認される一方，○の外側で増加したり減少したりしている化合物があることがわかる．GSHの直下にGSHと同等の泳動時間で質量数がわずかしか違わない未知物質が著明に増加しているのが確認できる．Soga T, et al: J Biol Chem (2006) 281: 16768-16776 より改変．

はCOの添加によって部分的に抑制がかかることが明らかになった[7]．以上の結果から，COがNOとは不可分の生物作用を持ち，特異的な生理作用を発揮するメディエーターであることを示すためには，特異的なレセプター探索をすることが不可欠となった．

Ⅱ．メタボローム解析技術によるCOの標的分子の探索

これまで報告されてきたCOの生物作用は主にsGCの活性化，K^+チャネルの開口確率の増加に伴う細胞膜の過分極，およびMAPキナーゼの活性化であるが，後者2つの作用はCOが結合する分子の実態が明らかにされていない点で，COによる特異的情報伝達系であるか否かは不明である．COがsGC以外のヘム酵素に結合して細胞機能を調節する可能性はないか？ また哺乳類ではNOで作動せず，COで作動する特異的なスイッチは存在しないか？ この問題を解決するためにメタボローム解析法を応用し，候補分子の1つとしてメチオニンからシステインへの代謝律速酵素であるシスタチオニンβ合成酵素（CBS）を同定するに至った（図5）．この酵素はピリドキサルリン酸の酵素活性中心の近傍にヘムが存在するものの，ヘム自身は酵素反応の実行に関わらないため，長くその機能は不明であった．この酵素には数μMレベルのCOで阻害がかかる一方，NOでは阻害がかからないことが*in vitro*で明らかになったのである．

病態時におけるCOの増加が起こる実験モデルとして，筆者らはアセトアミノフェンによるマウスの肝障害モデルを用いて検討を行った．アセトアミノフェンは硫酸抱合，グルタチオン抱合などにより代謝されるが，過剰量を投与するとシトクロムP450で代謝され，毒性の高い中間代謝産物であるNAPQIが生成される．この化合物はP450自身をも攻撃し，酵素活性を失ったP420が生成されることが知られている[9]．P420のヘムはタンパク質への結合が脆弱なため，HOの基質としてCO増加が容易に起こるようになる．このような状況では既知物質としてメチオニンやS-アデノシルメチオニンの増加，ホモシステインの増加，グルタミン酸，グルタミンの低下，酸化型・還元型グルタチオンの低下が確認される一方，○の外側で増加したり減少したりしている化合物があることが判明した．図5に示すように，GSHの直下にGSHと同等の泳動時間で質量数がわずかしか違わない未知物質が著明に増加しているのが確認できるが，これを分取分析したところGSHのシステインが2-アミノ酪酸に置き換わったオフタルミン酸であることが判明した[8]．

アセトアミノフェン投与時に起こるメチオニンやホモシステインの増加反応はCOの生成を抑制するHOの阻害剤を投与すると略完全に抑制されたことから，筆者らはホモシステインとそれ以下のトランススルフレーション経路との境界にあり，トランススルフレーションの律速酵素であるCBSに着目し，この組換え型酵素を用いて，μMオーダーの生理的レベルでのCOによる阻害がかかること，NOでは阻害がかからないことを明らかにした（データ未発表）．すなわち，本酵素はCOが特異的に効果を示すガスセンサーであることが示唆された．肝臓におけるHOを介したCOの増加を介して，その生成産物であるシステインや，トランススルフレーション

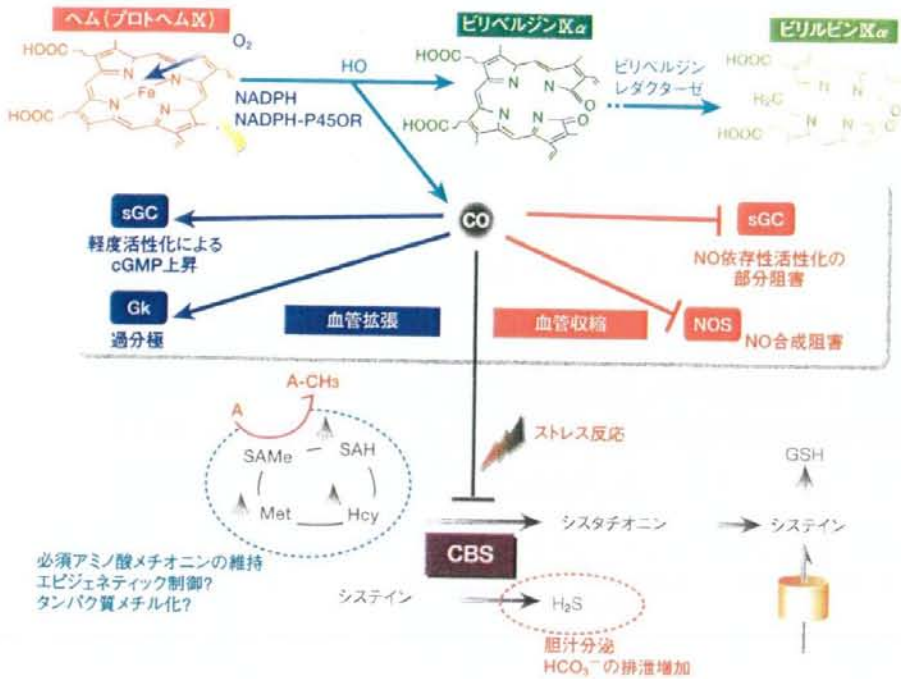

図6. COによるCBSの阻害と生理機能の制御

COがストレスで増加するとCBSを阻害し，肝臓実質ではH_2Sを低下させることにより胆汁中のHCO_3^-の排泄を増加させる一方，メチオニンプールを確保し，リメチレーション回路の代謝流量を増やすことによってタンパク質のメチル化を惹起することが明らかになった．

経路の終末生成物である硫化水素（H_2S）が減少し，その結果，HCO_3^-の分泌を増加させていることによるものであることも合わせて明らかになった．このような胆汁分泌機能の制御作用はCBSを欠失したマウスでは消失する（データ未発表）．以上の成績はCOがsGC以外のシステムを使って細胞機能を制御すること，およびH_2S自身が第3のガスメディエーターであることの可能性を示唆するものである．

おわりに

COのようなガス分子は極小分子であり，代謝経路に対する作用をCE-MSを用いて系統的に探索し，仮説を立てることによりその標的分子を見いだすことができた．酵母two-hybridシステムやアフィニティーナノビーズでレセプター分子を吊り上げることはガス分子では不可能であり，メタボロミクスを用いてガス分子に応答して変動する代謝経路に着目し，標的探索域を狭めて候補分子を挙げていく手法により新しい代謝制御機構の探索が可能である．今後，ストレス誘導性のCOによってメチル化を受けるタンパク質・生体高分子の同定を進めることによりガス分子を介した代謝制御のみならず，細胞機能制御機構の探索も推進されるものと思われる．

謝辞　本稿の図5の成績を得るにあたり，慶應義塾大学先端生命科学研究所の曽我朋義教授およびRichard Baran氏に協力をいただきました．心より深謝いたします．

文献

1) Tian J, et al: Proc Natl Acad Sci USA (2005) 102: 10670-10675
2) Suematsu M, et al: Biochem Biophys Res Commun (1994) 205: 1333-1337
3) Suematsu M, et al: J Clin Invest (1995) 96: 2431-2437
4) Goda N, et al: J Clin Invest (1998) 101: 604-612
5) Suematsu M, et al: Hepatology (2000) 31: 3-6
6) Ishikawa M, et al: Circ Res (2005) 97: e104-e114
7) Kajimura M, et al: FASEB J (2003) 17: 506-508
8) Soga T, et al: J Biol Chem (2006) 281: 16768-16776
9) Mori M, et al: Hepatology (1999) 30: 160-168

Hiromichi Ishikawa
Tomoaki Naito
Toshihiko Iwanaga
Hiromi Takahashi-Iwanaga
Makoto Suematsu
Toshifumi Hibi
Masanobu Nanno

Curriculum vitae of intestinal intraepithelial T cells: their developmental and behavioral characteristics

Authors' address
Hiromichi Ishikawa[1], Tomoaki Naito[1,2], Toshihiko Iwanaga[3], Hiromi Takahashi-Iwanaga[3], Makoto Suematsu[2], Toshifumi Hibi[4], Masanobu Nanno[5]
[1]Department of Microbiology and Immunology, Keio University School of Medicine, Shinjuku-ku, Tokyo, Japan.
[2]Department of Biochemistry and Integrative Medical Biology, Keio University School of Medicine, Shinjuku-ku, Tokyo, Japan.
[3]Laboratory of Cytology and Histology, Graduate School of Medicine, Hokkaido University, Kita-ku, Sapporo, Japan.
[4]Department of Internal Medicine, Keio University School of Medicine, Shinjuku-ku, Tokyo, Japan.
[5]Yakult Central Institute for Microbiological Research, Kunitachi, Tokyo, Japan.

Correspondence to:
Hiromichi Ishikawa
Department of Microbiology and Immunology
Keio University School of Medicine
35 Shinanomachi, Shinjuku-ku
Tokyo 160-8582, Japan
Tel.: 81 3 5363 3766
Fax: 81 3 5360 1508
E-mail: h-ishika@sc.itc.keio.ac.jp

Acknowledgements
We would like to thank all members of our laboratories who have contributed to portions of our work embodied in this review paper. The data provided in the preparation of this review were supported in part by a Grant-in-Aid for Creative Scientific Research, the Japan Society for the Promotion of Science (13GS0015), by Special Coordination Funds for Promoting Science and Technology from the Japanese Ministry of Education, Culture, Sports, Science and Technology, by Research on Specific Diseases, Japanese Ministry of Health, Labor and Welfare, and by Keio University Special Grant-in-Aid for Innovative Collaborative Research Projects (T.H.). T.N. is a research fellow supported by the 21st Century Center-of-Excellence Program for Life Science from MEXT (M.S.).

Immunological Reviews 2007
Vol. 215: 154–165

Immunological Reviews
0105-2896

Summary: The alimentary tract has an epithelial layer, consisting mainly of intestinal epithelial cells (IECs), that is exposed to the exterior world through the intestinal lumen. The IEC layer contains many intestinal intraepithelial T cells (IELs), and the total number of IELs constitutes the largest population in the peripheral T-cell pool. Virtually all γδ-IELs and many αβ-IELs in the mouse small intestine are known to express CD8αα homodimers. A wide range of evidence that supports extrathymic development of these CD8αα$^+$ IELs has been collected. In addition, while several studies identified cells with precursor T-cell phenotypes within the gut epithelium, how these precursors, which are dispersed along the length of the intestine, develop into γδ-IELs and/or αβ-IELs has not been clarified. The identification of lymphoid cell aggregations named 'cryptopatches' (CPs) in the intestinal crypt *lamina propria* of mice as sites rich in T-cell precursors in 1996 by our research group, however, provided evidence for a central site, whereby precursor IELs could give rise to T-cell receptor-bearing IELs. In this review, we discuss the development of IELs in the intestinal mucosa and examine the possibility that CPs serve as a production site of extrathymic IELs.

Keywords: CD8αα$^+$-IEL, γδ-IEL, αβ-IEL, extrathymic development of IEL, cryptopatches

Introduction

Surfaces in the body in contact with the outside world include the epidermis and the mucous epithelia. Directly below both the epidermis and the mucous epithelia is an extensive basement membrane (Bm) that serves as a thin wall separating them from the interior of the body, and no capillaries or lymphatic vessels are present in the epidermis and mucous epithelia. Therefore, any lymphomyeloid cells distributed in epidermis and mucous epithelia are extravasated from the postcapillary venules in the interior of Bm, and they must move into the epidermis and mucous epithelia by crossing Bm. T cells and B cells evolved as key players in the immune system of vertebrates, and an infinite number of antigen-specific receptors are produced by a mechanism called somatic gene rearrangement. It has been known for some time that lymphocytes are distributed in the epidermis and mucous epithelia, and in about the middle of the 1970s, it became clear that most intestinal intraepithelial lymphocytes settling in the small intestine of mice are T cells [intestinal

intraepithelial T cells (IELs)] (1). Furthermore, almost all T cells in the epidermis of laboratory mice are those expressing homogenous γδ-type T-cell receptors (TCRs), also known as dendritic epidermal T cells (DETCs). The surprising finding concerning these γδ-DETCs is that they are produced in the thymus at about day 15 of embryonic life and are thus derived from the first wave of fetal γδ thymocytes (2). In this review article, we focus our discussion mainly on findings obtained in mice concerning development of IELs distributed among intestinal epithelial cells (IECs).

Surprising evidence, showed by studies using a monoclonal antibody to TCR, is that almost all mouse IELs are T cells (3–9). IELs are radically different from T cells residing in other sites of the body; most of them are ill-defined T cells with unusual but distinctive characteristics. These cells are located at the front line of defense, at the point which the interior of the body comes in contact with the greatest numbers of antigens from the exterior world.

The interior of the Bm consists of *lamina propria* (LP) that contains abundant immunoglobulin A $(IgA)^+$ B cells, $CD3^+$ T cells (Fig. 1), and various lymphomyeloid cells. In contrast (as discussed later), the exterior of the Bm contains an IEC layer with prominent colonization of CD8α-expressing T cells (Fig. 1). The marked differences between the inside and the outside of the Bm are very important in connection with clarification of *in vivo* physiological functions and development of IELs on the front line of the intestinal mucosa. Research over the past 30 years has shown that IELs in mice and humans, especially those in the small intestine of mice, are a phenotypically and functionally distinctive subpopulation of peripheral T cells that is distinguished from so-called proper T cells, which are distributed in peripheral lymphoid tissues such as the spleen and lymph nodes (LNs) after development in the thymus (10). A vast majority of T cells found in peripheral lymphoid tissues of mice and humans are αβ T cells, while only a few γδ T cells are present. In contrast, IELs in mice and humans include large numbers of cells expressing αβTCRs and those expressing γδTCRs. From a study of IELs in athymic (nu/nu) mice, it is clear that many γδ-IELs are present, although the population size is decreased. In addition, in spite of the sharp decrease in αβ-IELs, meaningful numbers of these cells can be detected. Thus, a substantial proportion of γδ-IELs seems to be generated and/or expanded in the absence of the thymus. In contrast, it is well known that both γδ T cells and αβ T cells are virtually undetectable in the spleen and LNs of nu/nu mice (11, 12). Functional aspects of IELs have been adequately explained in other reviews in this volume, and this review contains personal insights concerning the past, present, and future of extrathymic development of IELs and where the research is heading. Furthermore, we discuss how IELs settle down in the IEC layer through Bm and emphasize how they behave and survive in the IEC layer in situ.

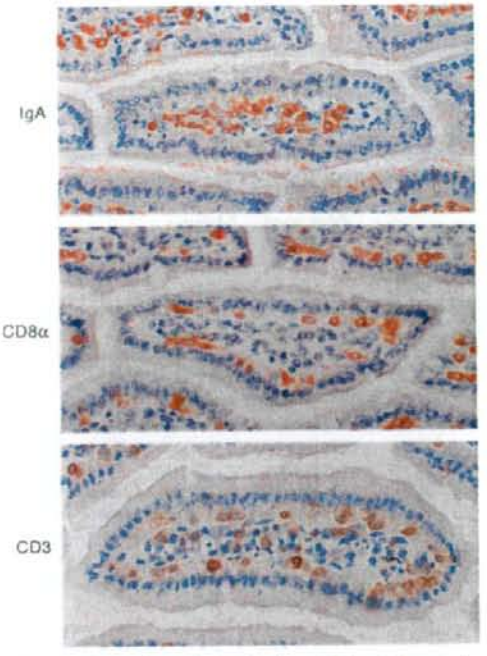

Fig. 1. Immunohistochemical visualization of IgA-, CD8α-, and CD3-expressing cells in jejunal villi. Note that IgA^+ B cells are localized exclusively in the LP, whereas that $CD8\alpha^+$ T cells, namely intestinal IELs, are compartmentalized above the Bm in the IEC layer of the small intestine. In contrast, in addition to numerous IELs in the IEC layer, $CD3^+$ T cells, mostly $CD4^+$ T cells, are also found in the LP of the villi.

IEL development in the intestinal epithelium: evolutionary perspective

The intestine was the first organ to appear when animals became multicellular; even though some multicellular animals lacked brains, there were none without intestines. To defend the intestines against pathogenic microorganisms and harmful substances from the exterior, macrophage-like lymphoid cells developed directly under the intestinal epithelium. The first organ to appear in our living body is the primordial gut, and many organs, including lungs, liver, pancreas, and thyroid gland, are derived from this apparatus. Some marine animals breathe through gills that develop from the upper digestive tract, and pulmonary respiration evolved with the change from marine to terrestrial life. It is well known that the thymus was derived from part of the gill. Therefore, all these organs have

a kindred relation, and latent production of lymphocytes appears possible. In agreement with this argument, fetal liver of mammals including mice is a primary lymphoid organ producing lymphomyeloid cells.

The IEC layer was proposed as a lymphocyte-producing organ as early as 1967 (13). Gut-associated lymphoid tissue (GALT), which contains about 60% of all peripheral lymphocytes, monitors and defends the intestinal mucosa in most vertebrates. T cells and antibodies, the key players in adaptive immunity, have not been found in the jawless fish *Agnatha*, the oldest phylogenic vertebrate lacking a thymus, spleen, and LNs (14, 15). However, GALT, characterized by many lymphoid cells, is found in *Agnatha* such as lampreys and hagfish, and the intestinal mucosa of such animals appears to serve as lymphocyte production sites (14, 15). Furthermore, the bursa of Fabricius, a GALT of birds, and Peyer's patches (PPs) of ruminants are also well known as primary lymphoid tissues responsible for the development of B cells (16). If we consider the large amount of knowledge based on animal evolution, there is nothing remarkable about development of IELs in intestinal mucosa *in situ* in mice and humans.

Findings supporting extrathymic development of murine IELs

Type a and type b IELs

IELs of the murine gut have been identified as ill-defined T cells that lurk in the anatomical front of the intestine (1, 3–9), with a primarily cytotoxic T-cell phenotype (4, 17–19). A large fraction of murine IELs bearing CD8αα homodimers ($CD8\alpha\alpha^+$ IELs) have been proposed to originate locally through a differentiation process initiated in c-kit$^+$IL-7R$^+$lineage marker $(Lin)^-$ gut precursors. Hayday et al. (10) have proposed that the functional complexity and phenotype heterogeneity of IELs might be simplified if IELs are classified into just two cell types: 'a' and 'b'. Type a includes $CD4^+$ and $CD8\alpha\beta^+$ αβ-IELs that primarily recognize antigens presented by classical major histocompatibility complex (MHC) class I and class II molecules and are primed within the systemic circulation. Type b IELs include $CD8\alpha\alpha^+$ αβ- and γδ-IELs that respond to antigens not restricted by classical MHC molecules. Although $CD8\alpha\alpha^+$ αβ- and γδ-IELs are clearly different from one another, type b IELs share many 'unconventional' features that distinguish them from type a IELs.

Although dependence of the type a $CD8\alpha\beta^+$ and type b $CD8\alpha\alpha^+$ αβ-IELs but not type b $CD8\alpha\alpha^+$ γδ-IELs on MHC class I molecules was reported using β2-microglobulin (β2m)-deficient mice (20, 21), a recent analysis of gene expression profiles between type b $CD8\alpha\alpha^+$ αβ– and γδ-IELs showed a high degree of similarity (22). These two classes of IELs are not only related functionally but also have a kindred relation.

The total number of αβ-IELs decreased sharply in $\beta2m^{-/-}$ mice due to the disappearance of both $CD8\alpha\beta^+$ (type a) and $CD8\alpha\alpha^+$ (type b) subsets. In β2m/TCR-δ double-mutant mice, which lack β2m and γδ-IELs, the $CD8\alpha\alpha^+$ subset expanded dramatically, while the $CD8\alpha\beta^+$ subset did not (Fig. 2). Thus, in the absence of γδ-IELs, αβ-IELs in β2m-deficient mice outnumbered those in wildtype littermates due to considerable expansion of type b $CD8\alpha\alpha^+$ αβ-IELs (Fig. 2). These results (23) indicate that generation of type b $CD8\alpha\alpha^+$ αβ- and γδ-IELs is essentially β2m independent, while generation of type a $CD8\alpha\beta^+$ αβ-IELs is highly dependent on β2m-MHC class I

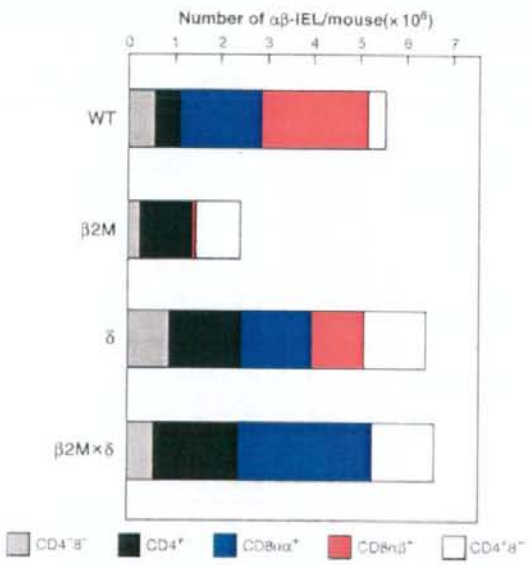

Fig. 2. Composition of αβ-IEL subsets in wildtype (WT), β2m-deficient, TCR-δ mutant (δ), and β2m × TCR-δ double-mutant (β2m × δ) mice. These four different mice were littermates of the F_2 generation of an intercross between $\beta2m^{-/-}$ and $\delta^{-/-}$ mice. IELs isolated from these mutant mice were incubated first with anti-CD8α monoclonal antibody (biotinylated) and then with streptavidin–allophycocyanin. After washing, the IELs were counterstained with two combinations of two phycoerythrin-conjugated monoclonal antibodies (anti-CD4 and anti-CD8β) and two fluorescein-isothiocyanate-conjugated monoclonal antibodies (anti-αβ TCR and anti-γδ TCR, respectively). Absolute numbers of double-negative ($CD4^-CD8^-$), single positive ($CD4^+$, $CD8\alpha\alpha^+$, or $CD8\alpha\beta^+$), and double positive ($CD4^+CD8^+$) subsets in the αβ-IEL population were calculated on the basis of total number of αβ-IELs. Note that $CD8\alpha\alpha^+$ and $CD8\alpha\beta^+$ αβ-IEL subsets are absent from the small intestine of β2m mutant mice, whereas the $CD8\alpha\alpha^+$ but not $CD8\alpha\beta^+$ αβ-IEL subset expands markedly in the small intestine of double-mutant β2m × δ mice, namely β2m mutant mice that lack γδ-IELs.

molecules expressed by the controlling cells at the type a IEL precursor development site. These findings suggest the possibility that type b IELs, CD8αα$^+$ αβ- and γδ-IELs, develop in the same anatomical site(s). When no β2m-MHC class I molecules are present, development of CD8αα$^+$ αβ-IELs is likely inhibited because development of CD8αα$^+$ γδ-IELs surpasses that of CD8αα$^+$ αβ-IELs competitively.

CD8αα exerts a specific and high affinity for interaction with the non-classical MHC class I molecule thymus leukemia (TL) antigen, which is expressed abundantly by murine thymic stromal cells and by IECs (24). It was also proposed that CD8αα$^+$ TCR-αβ T cells originated from the thymus through agonist-dependent positive selection (25). The mechanism of development of CD8αα$^+$ T cells and in vivo physiological functions, including whether or not this scenario is correct, remain to be clarified.

Evidence obtained in a study of athymic *nu/nu* mice

The evidence that most clearly supports thymus-independent development of gut-oriented type b IELs is obtained from a study of T cells in the athymic (nu/nu) mouse. Almost no γδ T cells or αβ T cells are observed in the spleen and LNs of nu/nu mice. A considerable population of γδ-IELs is present in IELs of nu/nu mice, and αβ-IELs can also be detected (Fig. 3). Since these αβ-IELs are CD8αα$^+$ type b IELs and no αβ-IELs are found in TCRβ$^{-/-}$ mice (Fig. 3), it is evident that a few type b αβ-IELs develop independently of the thymus.

Many reports have been published on the thymus-independent development of type b IELs. These findings include the presence of a few CD3$^-$ lymphocytes in the IELs and the resulting possession of precursor T-cell-like properties, i.e. the fact that these tentative precursors observed in mice and humans retain messenger RNA (mRNA) for recombination-activating gene-1 (RAG-1) and RAG-2 and pre-Tα molecules. For details, the reader is referred to previously published articles (8, 9, 26–30).

Here, we introduce our results (31) from screening lymphoid tissues of athymic (nu/nu) RAG-1$^{GFP/+}$ animals, which have the green fluorescence protein (GFP) gene in the RAG-1 locus. Only CD19$^+$ B cells (32) in the bone marrow (BM), spleen, mesenteric lymph nodes (MLNs), and PPs express RAG-1, while in IELs, a meaningful number of CD19$^-$ cells express RAG-1, although the amount of RAG-1 molecules expressed is low (Fig. 4). Since CD19$^-$RAG-1^{low} IELs are CD3$^-$ and are not observed in IELs of RAG-1$^{+/+}$ mice, this finding supports the distribution of small numbers of RAG-1^{low} precursor T cells in IELs. DETCs of wildtype mice that express homogenous γδTCRs (Vγ5Jγ4Cγ1 and Vδ1Jδ2Cδ) are known to be derived from the first wave of fetal γδ thymocytes, which are produced in the thymus at about antenatal day 15 (2). Therefore, even though Vγ5$^+$ DETCs are not present naturally, it has been shown that Vγ1/Vδ6$^+$ DETCs are present in the epidermis of nu/nu mice (33). These findings together with those reported by Matis et al. (34) and Yoshikai et al. (35) prove that the thymus-dependent type a subset (2) and the thymus-independent type b subset (33–35) such as γδ T cells are present in peripheral anatomical sites other than the IEC layer.

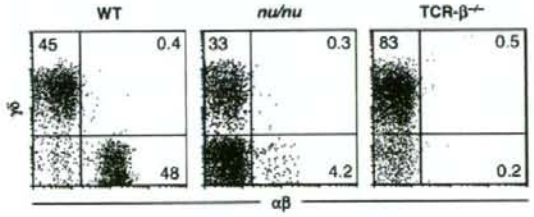

Fig. 3. Composition of αβ- and γδ-IELs isolated from wildtype (WT), athymic (nu/nu) and TCR-β$^{-/-}$ mice. Flow cytometric analysis of IELs isolated from five individuals each of three different strains of mice was performed, and the representative profiles of IELs are presented. In this case, absolute numbers of IELs recovered were 5.4×10^6 from WT mice, 2.3×10^6 from nu/nu mice, and 5.3×10^6 from TCR-β$^{-/-}$ mice. The percentage of αβ- and γδ-IELs in the corresponding quadrants is shown. Note that αβ-IELs are drastically reduced in the athymic condition. Nevertheless, a meaningful number of αβ-IELs are still present in the small intestine of the nu/nu mouse compared with the total absence of αβ-IELs from the TCR-β$^{-/-}$ mouse. In contrast, there are few, if any (<1%), αβ T cells in the spleen and MLNs of this same nu/nu mouse (data not shown).

A new member of GALT: cryptopatches

Discovery of cryptopatches in mouse small intestine as the precursor IEL-producing site

We have shown that multiple tiny lymphoid cell aggregations, filled with about 1000 closely packed c-kit$^+$IL-7R$^+$Thy1$^+$ CD3$^-$B220$^-$ lymphocytes, colonize throughout the small intestinal mucosa of C57BL/6 mice (36). The location is in the crypt LP [cryptopatches (CPs)]. They are first detected in the third week of postnatal life in C57BL/6 mice. In terms of morphogenesis, cellular composition, and fine tissue structure, neither PPs nor isolated lymphoid follicles (ILFs) are identical to CPs (30, 37). CPs contain neither cells undergoing apoptosis nor cells bearing RAG-1 molecules but do contain dendritic stromal cells bearing CD11c/CD18 molecules. The presence of transcripts for germ line TCR genes and mRNA for proteins involved in TCR rearrangement (38) and the ability of c-kit$^+$Lin$^-$ CP cells to generate TCR$^+$ IELs in T-cell-deficient mice (39) indicate that at least some CP cells are committed to the T-cell lineage and are competent for generation of

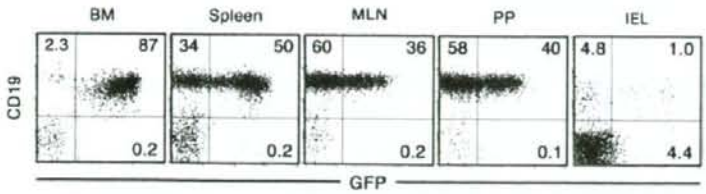

Fig. 4. A small number of RAG-1-expressing lymphocytes are present in the intestinal intraepithelial compartment of *nu/nu* mice. Lymphocytes from BM, spleen, MLNs, PPs, and IEC layer (IELs) were isolated from *nu/nu* mice carrying a GFP gene in place of the *RAG-1* gene (*nu/nu* RAG-1$^{GFP/-}$ mice) (31) and then were subjected to flow cytometric analysis. Note that only in the IEL preparation, a meaningful number of GFP-dull-positive cells are present. Importantly, these cells are not B-lineage cells because they are CD19 negative.

thymus-independent type b IELs, especially CD8αα$^+$ γδ-IELs (12).

To obtain direct evidence for generation of type b IELs from the precursors that settle in CPs, cytokine receptor γ chain mutant *nu/nu* mice that lack a thymus, PPs, CPs, and intestinal T cells (40) were reconstituted with wildtype Ly5.1$^+$ BM cells. BM-derived TCR$^-$ IELs first appeared within villous epithelia of small intestine overlaying regenerated CPs, and these TCR$^-$ IELs subsequently emerged throughout the epithelia. Thereafter, TCR$^+$ IELs increased sluggishly to a number comparable with that in athymic *nu/nu* mice and consisted of both αβ- and γδ-IELs (38). Taking all these results together, CPs are the first murine GALT to be identified that most likely serve as the site of development of lymphohemopoietic precursors for type b IEL descendents at commencement of weaning (36, 38, 40). Recent data showed a clonal relationship between CP T cells and γδ-IELs (41).

Evidence that CPs are not the precursor IEL-producing site

By characterizing phenotypically distinct lineage-negative populations in the CPs and gut epithelium, Lambolez *et al.* (42) showed that only 3% of CP cells were clearly involved in T-cell differentiation and suggested that these CP structures may have an additional physiological role in the gut. In contrast, Guy-Grand *et al.* (43) clarified the following from an examination of RAG-2 expression using GFP transgenic mice evaluated by GFP (carrying a *GFP* reporter gene driven by the RAG-2 promoter). In *nu/nu* mice, T lymphopoiesis occurs mainly in MLNs, less in PPs, and not in CPs. Importantly, this extrathymic T lymphopoiesis is totally repressed in euthymic mice (43). Based on these findings, Guy-Grand *et al.* (43) concluded that in normal euthymic mice, all gut αβ-IELs, including type b CD8αα$^+$ αβ-IELs, are of thymic origin. It has also been shown that thymus transplantation into *nu/nu* mice results in the appearance of thymus graft-derived αβ- and γδ-IELs in *nu/nu* recipients (44). To evaluate this important issue, we generated *nu/nu aly/aly* (*alymphoplasia*) double-mutant mice lacking thymus, all LNs, PPs, and ILFs but possessing CPs (12). Substantial colonization by γδ-IELs comprising the major CD8αα$^+$ subset took place, and use of TCR-γ-chain variable gene segments by these γδ-IELs was unaltered (12). These findings indicate that MLNs and PPs are not an absolute requirement for development of γδ-IELs but instead support the notion that gut CPs generate progenitor γδ-IELs, even under athymic conditions. However, absolute numbers of γδ-IELs from *nu/nu aly/aly* mice are smaller than those from the corresponding control *nu/nu* mice (12). These features indicate that LNs and PPs in fact determine the number of γδ-IELs under the *nu/nu* conditions. In any event, there would be a hierarchy of T-cell production in terms of anatomical sites, although the detailed mechanism is still not well understood. By a mechanism such as the tropic effect of thyrotropin-releasing hormone on IEL development (45, 46), however, almost all αβ-IELs appear to originate in the thymus in euthymic mice. In *nu/nu* mice, however, IELs appear to be generated mainly by the MLNs and PPs, and in *nu/nu aly/aly* mice that lack a thymus, all LNs, PPs, ILFs, and αβ- and γδ-IELs appear to be generated from other anatomical sites, probably CPs. In this context, it has been reported that T-cell-committed precursors are distributed not only in the thymus but also in the BM, liver, and spleen (47–49). It is inferred based on these findings that extrathymic T-cell generation has not been proven to be repressed completely in normal euthymic mice. In other words, there is no solid evidence denying a possibility that extrathymic T cells are generated in euthymic conditions.

It has recently been shown that retinoic acid-related orphan receptors (RORγt) detected in fetal lymphoid tissue-inducer (Lti) cells are also expressed in cells within gut CPs and that, by fate mapping of RORγt$^+$ cells, type b IELs, such as γδ-IELs, are not the progeny of RORγt$^+$ CP cells (50). However, it remains an open question whether a small fraction of lymphoid cells in CPs does not express RORγt or all CP cells express RORγt. To investigate this point in detail, we generated *nu*/+ RORγt$^{GFP/+}$

mice and nu/nu RORγt$^{GFP/+}$ mice and obtained the results shown in Fig. 5.

In agreement with the report of Eberl and Littman (50), many RORγt^{+} (GFP^{+}) cells were present in thymocytes from nu/+ RORγt$^{GFP/+}$ mice, although GFP expression was weak (unpublished observation). Analysis of CP cells from nu/nu RORγt$^{GFP/+}$ mice showed that almost all GFP^{+} cells were interleukin-7 receptor positive (IL-7R)$^{+}$ and CD8α^{-}. However, CD3^{-} cell subsets showing various phenotypes such as IL-7R^{+}GFP^{-}, c-kit^{+}GFP^{+}, c-kit^{+}GFP^{-}, c-kit^{-}GFP^{+}, Thy-1^{+}GFP^{+}, Thy-1^{+}GFP^{-}, Thy-1^{-}GFP^{+}, CD4^{+}GFP^{+}, CD4^{+}GFP^{-}, CD4^{-}GFP^{+}, CD8^{+}GFP^{-}, Lin^{+}GFP^{+} (majority of them CD4^{+}GFP^{+}), Lin^{+}GFP^{-}, and Lin^{-}GFP^{+} were all present but with variable population sizes (Fig. 5A). In addition to the colonization of γδ-IELs and small numbers of αβ-IELs, of particular note was the presence of CD3^{-} IELs showing c-kit^{+}GFP^{+} and IL-7R^{+}GFP^{+} phenotypes in IEC compartments of nu/nu RORγt$^{GFP/+}$ mice (Fig. 5B). These new findings do not necessarily support the conclusion of Eberl and Littman (50) and show distribution of RORγt^{-} c-kit^{+}, IL-7R^{+}, Thy-1^{+}, CD4^{+}, CD8^{+}, and/or Lin^{+} lymphocytes in murine gut CPs. In this context, we previously reported (36) that CPs are not detectable in IL-7R$^{-/-}$ mice. However, although γδ-IELs are absent owing to selective blockage of TCR-γ gene rearrangements (51), we noticed only a slight decrease in development of type b αβ-IEL subsets in IL-7R$^{-/-}$ mice. With these observations in mind, we reinvestigated hundreds of cryosections prepared from small intestines of IL-7R$^{-/-}$ mice by immunohistochemistry and verified that conspicuously emaciated CPs filled with c-kit^{+} cells and decreased by more than 16-fold in number were present in this mutant intestine (40). Similarly, although mice genetically deficient in lymphotoxin α (LTα) have been reported to lack CPs (52), we observed that histogenesis of CPs and intestinal development of αβ- and γδ-IELs remained almost intact in LTα$^{-/-}$ mice (37). In consideration of our research results, i.e. CPs are observed not only in IL-7R$^{-/-}$ mice but also in LTα$^{-/-}$ mice, the conclusion that CP development is not found in RORγt$^{GFP/GFP}$ mice lacking RORγt (50) seems to require careful reexamination. It is easy to ascertain the presence of CPs, but it is quite difficult to conclude that CPs are totally absent. At the same time, we should examine if type b IELs, such as γδ-IELs, develop from the RORγt^{-} c-kit^{+}GFP^{-} or IL-7R^{+}GFP^{-} subset (Fig. 5A) distributed in the CPs of nu/nu RORγt$^{GFP/+}$ mice.

What are these CPs?

Based on the results obtained using RORγt$^{GFP/+}$ mice, Eberl and Littman (50) proposed that the principal function of murine c-kit^{+}Lin^{-} RORγt^{+} CP cells is to induce formation of lymphoid

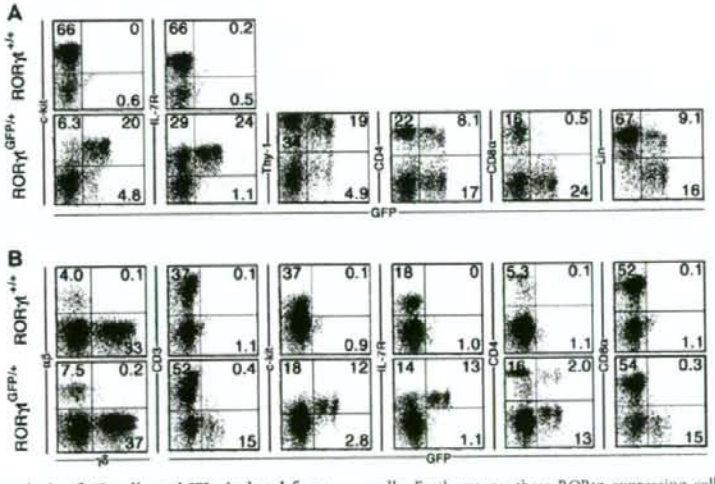

Fig. 5. Flow cytometric analysis of CP cells and IELs isolated from nu/nu mice carrying the wildtype RORγt genes (RORγt$^{+/+}$ mice) and carrying a GFP gene in place of RORγt gene (RORγt$^{GFP/+}$ mice). CP cells were isolated according to the method described previously (37). Although CP cells (A) and IELs (B) isolated from nu/nu RORγt$^{+/+}$ mice do not contain GFP^{+} cells, those isolated from nu/nu RORγt$^{GFP/+}$ mice contain a substantial population of GFP^{+} RORγt-expressing cells. Furthermore, these RORγt-expressing cells from CP and IEL compartments of nu/nu RORγt$^{GFP/+}$ mice appear to be composed of two discrete RORγt^{high} and RORγt^{low} cell subsets. 'Lin' in A represents lineage markers CD3, B220, Mac-1, Gr-1, TER119, CD11c, CD4, and CD8α. Lymphocytes isolated from spleen, MLNs, and PPs of nu/nu RORγt$^{GFP/+}$ mice lack GFP^{+} RORγt-expressing cells (data not shown).

follicles, namely ILFs, in the LP in a manner similar to induction of LNs and PPs by RORγt$^+$ LTi cells. It is also possible that CP cells are precursor cells of gut-oriented lymphomyeloid cells other than IELs (42). The CPs of mice have been discounted as the anatomical site where precursor IELs congregate, as no CP-like lymphoid clusters have been reported in the intestinal mucosa of mammals other than mice. However, since evidence indicates development of gut-oriented T cells, mainly IELs, in the intestinal mucosa of humans (53–59) and rats (60), to determine whether or not CPs and CP-like lymphoid tissues are present in enteric mucosa of animals is an important goal for future experiments. We (61) showed that lymphocyte clusters, just like the structure named lymphocyte-filled villi (LFV) (62), populated predominantly with c-kit$^+$IL-7R$^+$ cells and less with αβTCR cells, were found distributed throughout the length of the small intestine of rats. Nevertheless, we were unable to verify whether these rat LFV, containing undifferentiated lymphocytes, represented clusters of extrathymic precursor T cells. With regard to this same issue, several groups have actively sought evidence of CPs in the human gastrointestinal tract, illuminating distinctive T-cell facets of human fetal gut lymphocytes (58, 59). In agreement with these findings, we have identified multiple tiny c-kit$^+$ lymphoid cell clusters in human fetal intestine at the second trimester of fetal life (unpublished observation). Overall, we take it for granted that the differentiation of type b IELs is not exactly the same among different vertebrates. For instance, if epidermal immune regulation by γδ-DETCs in mice is of considerable physiological importance, how do other mammals including humans cope without γδ-DETCs? In these animals, immunoregulatory function should be provided by some lymphoid cells other than γδ-DETCs.

Based on these findings, precursors of type b IELs that develop extrathymically in humans and rats appear to be produced in CP-like lymphoid tissues of mice during fetal life. Then, the precursors are dispersed throughout the LP or IEC layer, or self-renewal is localized in the IEC layer after expression of the αβTCR or γδTCR and completion of development, as in the case of B-1 B cells. Mouse DETCs (2) expressing homogenous Vγ5/Vδ1$^+$ γδTCRs are produced only in fetal thymus in a very limited period at about day 15 of fetal life. No such Vγ5/Vδ1$^+$ γδ-DETCs are found in the epidermis of athymic nu/nu mice (33), while homogenous Vγ5/Vδ1$^+$ γδ-DETCs of euthymic mice are present throughout life (1.5–2 years). If the supply of Vγ5/Vδ1$^+$ γδ-DETCs occurs only in the first wave of fetal γδ thymocytes development, the life of Vγ5/Vδ1$^+$ γδ-DETCs must be as long as the life of the mouse. Is this really the case? We do not think that it is. It is possible that precursor Vγ5/Vδ1$^+$ γδ-DETCs generated by fetal thymus at about day 15 of fetal life lurk somewhere in the body (such as in the epidermis or dermis), develop at a fixed pace, and produce new Vγ5/Vδ1$^+$ γδ-DETCs. It is also possible that γδ-DETCs expressing homogenous Vγ5/Vδ1-TCRs continuously undergo self-renewal in the epidermis. Indeed, γδ-DETCs are shown to recognize and respond to antigens expressed on damaged, stressed, or transformed keratinocytes by means of their TCRs and produce keratinocyte growth factors (63), and it has been indicated that continuous stimulation of Vγ5/Vδ1-TCR$^+$ γδ-DETCs by the relevant ligand(s) is critical for maintenance of γδ-DETCs throughout the life of animals (64). In this context, it is conceivable that extrathymically generated mature human and rat IELs, which originate from cells settling in CP-like lymphoid tissues of mice during fetal life, undergo continuous self-renewal over the entire postnatal life of these animals by stimulation with relevant gut-associated antigens. In conclusion, although much remains to be learned about the mysterious development of extrathymic T cells in general and also the enigmatic features of CPs before we evaluate them as anatomical sites in which murine type b precursor IELs develop, many aspects of extrathymic T-cell immunobiology are now coming together step-by-step.

Where do these IELs come from?

Many types of cells are present outside the Bm of the small intestine (Fig. 6). Cells other than IELs present in the IEC layer are known to develop from stem cells located in the crypt. As described in the Introduction, IELs must migrate into the IEC layer from LP across the Bm. Immunohistochemical examination has shown that there are at least 2, or many more, IELs for every 10 IECs in mouse small intestine (65, 66). Thus, absolute numbers

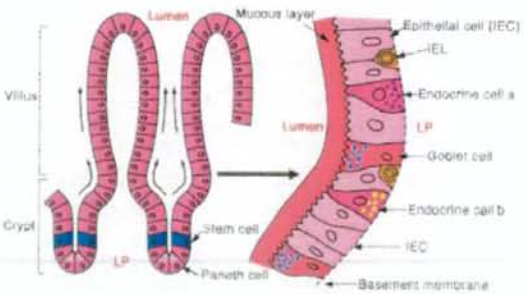

Fig. 6. Schematic illustration of cells that settle in the IEC layer of the small intestine. Every cell that settles in the IEC compartment, except IELs on the right of this figure (magnified), is the progeny of the stem cells shown on the left of this figure. Endocrine cells a and b contain different gut hormones.

of murine IELs are estimated to account for about half of the peripheral T-cell pool (67). However, it is not known if this huge IEL population enters the IEC layer across the Bm at sites such as crypts or villi, as shown in Fig. 6, or if IELs that have entered the IEC layer later cross the Bm and return to the LP. A large fraction of IELs is composed of γδ-IELs, and the fact that γδ T cells are almost absent from the LP compartment of villi in normal mice indicates that once they have entered the IEC layers, IELs and/or precursor IELs might return to LP in rare cases. By electron microscopy, we (39) showed that numerous lymphocytes cross the Bm that comes into contact with the CPs. Furthermore, by analysis of BM-chimeric mice, we (38) verified that donor BM-cell-derived IELs first appeared within the IEC layer of villi around regenerated CPs filled with BM-cell-derived c-kit$^+$ cells. These experimental results, in conjunction with a wide range of evidence showing the presence of small numbers of CD3$^-$ precursor IEL-like lymphocytes in the IEC compartment (8, 9, 26–30, 68), suggest a scenario in which precursor IELs that developed in CPs enter the IEC layer from the Bm that overlays CPs, and then these cells very sluggishly develop into mature type b IELs. In contrast, no definite findings have been obtained on whether type a αβ-IELs, such as CD4$^+$ or CD8αβ$^+$ T cells derived from the thymus, cross the Bm by some route and enter the IEC layer.

Parabiotic C57BL/6 Ly5.1 and Ly5.2 mice sharing circulation have been used by several groups (69, 70) to examine whether c-kit$^+$ stem cells that settle in local organs give rise to lymphoid cells in these organs in situ. As anticipated, the partner cells mixed rapidly in the spleen, all LNs, and PPs. In contrast, there were no or very few mixtures of partner cells in the thymus, CPs, and IELs (70). Poussier et al. (69) reported that IELs in the murine intestine did not mix together in parabiotic Ly5.1 and Ly5.2 mice. Overall, these findings appear to once again support the notion that IELs arise from their own pre-existing local precursor cells and that neighboring CPs continuously supply these local precursor cells at unknown rates.

What are these IELs?

There are still many riddles concerning the behavior and biological function of IELs that settle in the anatomical front of the IEC compartment in situ. Some of these unresolved issues are discussed below. We also discuss the development of research yet to be undertaken and future perspectives.

Behavior

Epithelial stem cells (Fig. 6) proliferate at the base of the crypts. Newly formed cells move upward and differentiate into various types of cells, mostly IECs (Fig. 6), in a process called migration-associated differentiation. The entire process of migration toward the top of the villi takes only several days, and the cells die there, most likely by apoptosis (71).

Electron microscopic examination of immersion-fixed tissue sections shows that IEL interdigitate tightly with IEC at the basolateral faces of IEC (Fig. 7A). Most IELs are terminally differentiated cells or those in the G0/G1 phase of the cell cycle.

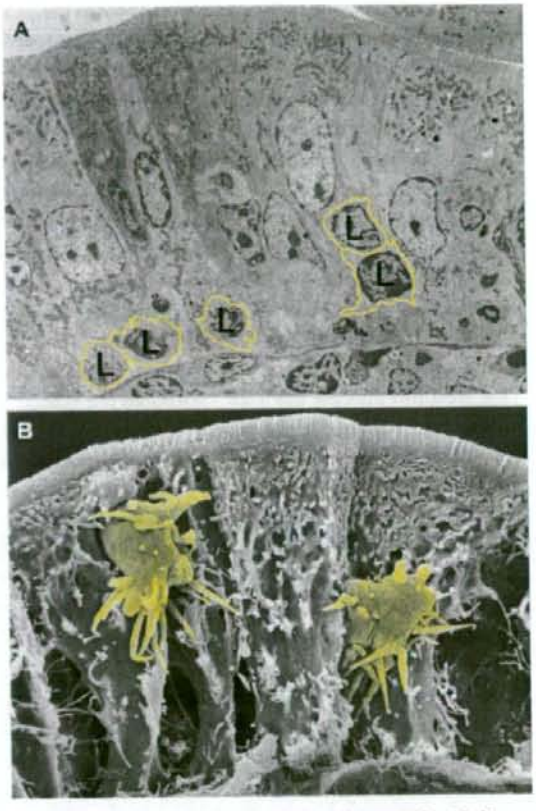

Fig. 7. Electron microscopic analysis of small intestinal epithelium. (A) Transmission electron micrograph showing IELs in intestinal epithelium obtained from an immersion-fixed sample. At least five IELs (L, edged with yellow line) are encased within the epithelium. No free space is visible among epithelial cells in the immersion-fixed samples; IELs appear to be tightly packed in the epithelium. (B) Scanning electron micrograph of IELs in a perfusion-fixed material. Two lymphocytes (yellow) equipped with spine-like processes are detected among epithelial cells. Note the broad free space at the basal region of the epithelium. A perfusion-fixed sample retains more precise and physiological three-dimensional structure of the tissues than that obtained by an immersion-fixed sample because the tissues shrink totally during and after the immersion-fixation. [This image is a modified reproduction of our figure that appeared in *Cell & Tissue Research*, used with kind permission of Springer Science and Business Media (83)].

It has been shown by bromodeoxyuridine labeling experiments that the average half-life of murine IELs is 3 weeks or much longer (72). If we assume that IELs are also migrating to the top of the villi, IECs must continuously get ahead of IELs, suggesting that individual IELs are capable of coming in contact with and/or surveying a significant number of IECs. Are IELs really migrating to the top of the villi? If so, at what speed are they migrating? At present, we do not know whether IELs can actually move upward or whether they maintain a rather stationary position.

Fig. 7B shows a vertically fractured face of perfusion-fixed small intestine by scanning electron microscopy. As is clear from this image, the surface in contact with intestinal lumen (apical surface of IEC) forms a tight junction between the IECs and is covered with microvilli with no gaps. However, there are relatively wide gaps between cells just on the Bm, and IELs are not always fixed by tight interdigitation with the lateral faces of the IECs. They appear to move to and fro relatively freely. IELs are also often in contact with IECs through process-like structures (*Fig. 7B*). In this image, it looks like the IELs are completely covered with trees, as if it were a mighty jungle viewed from the air, but there are considerable gaps near the ground under the trees where lions (≈ IELs) sleep and animals such as leopards (≈ IELs) lurk and move around (*Fig. 8*). In any case, clarification of the life and behavior of these mature IELs and the small number of precursor IELs in the IEC compartment are important topics for future study.

Fig. 8. A pictorial representation of the mighty jungle of the IEC layer. Based on the three-dimensional scanning electron microscopic picture of the IEC layer presented in *Fig. 7B*, we illustrated a mighty jungle in which a lion (≈IEL, with potentially cytotoxic function?) is resting on the ground (Bm) and a leopard (≈ IEL, like an indiscriminate predator?) is moving around a tree trunk (lateral face of IEC). It is evident that there is considerable room between the tightly packed treetop and the surface of the ground where these animals (≈ IELs) might be freely moving to and fro.

Oligoclonality

Whereas IELs are potentially able to use multiple Vβ TCR genes, both human (73–75) and murine (76) αβ-IELs are known to be derived from a limited number of oligoclonal T-cell clones. This oligoclonality of IELs points to the presence of a restricted set of foreign and/or self-antigens in the gut that may be ligands involved in the stimulation and expansion of these gut T cells. The large numbers of T cells distributed in the spleen and LNs appear to be inexperienced or virgin T cells that have not received antigen stimulation in normal specific pathogen-free mice. In contrast, T cells in the gut of specific pathogen-free mice are activated cells, continuously receiving antigen stimulation. As a result of selection, only competent clones expand and become dominant. Under these circumstances, even though the types of antigens are very diverse and are not limited to a restricted set of foreign and/or self-antigens, the TCR of αβ-IELs eventually results in oligoclonality. One mysterious and unexpected finding is that genetically identical individuals, even from the same litter and housed in the same cage, show distinct and apparently non-overlapping oligoclonal repertoires of both type a and type b αβ-IELs (76). Is the immune response to a diverse range of external antigens in the intestinal lumen really involved in the establishment of the oligoclonality of αβ-IELs? There is no firm experimental evidence to answer this question. In this respect, the finding that αβ-IELs in germ-free mice are also oligoclonal (77) is very intriguing and shows that αβ-IELs are oligoclonal, even when huge numbers of intestinal flora-derived antigens and microbe-associated immunoactive substances are not present.

Cytotoxicity

IELs are mostly terminally differentiated and activated T cells that possess a granular cytoplasmic structure containing perforin and granzyme (78), capable of killing Fc-receptor-bearing target cells after bridging them with anti-CD3, anti-αβTCR, or anti-γδTCR monoclonal antibodies (78–80). However, at most 10^7 IELs per mouse from the small intestine can be isolated for *in vitro* analysis, despite the fact that $5–10 \times 10^7$ IELs have been found to settle in the IEC compartment by immunohistochemistry (67) (*Fig. 1*). Therefore, we might have studied *in vitro* only a portion of the IELs, which can be isolated easily from intestinal mucosa as a subpopulation maintaining their typical granular cytoplasmic structure and cytotoxic activity. In this context, of great importance in the future is to examine *in vitro* characteristics of the large number of IELs that cannot be recovered using current techniques and/or are lost in the process of purification in a test tube. Such a 'missing' population should be examined,

if the cells maintain their characteristics of terminal differentiation. γδ-IELs from germ-free mice are known to show cytotoxicity (81) in the same way as αβ-IELs in germ-free mice show oligoclonality. Electron and light microscopy shows that murine IELs from scid/scid (severe combined immunodeficient) mice that are unable to generate αβ- and γδ-IELs have granulated IELs similar to those in normal mice (82), are $CD3^-CD8\alpha\alpha^+$ IELs are present in scid/scid mice and nu/nu scid/scid mice (40). In addition, findings showing that $CD3^-CD8\alpha\alpha^+$ IELs are not present in cytokine receptor γ chain mutant nu/nu mice lacking CPs (38, 40) suggest that a special but as yet unknown microenvironment in CP and IEC compartments could dictate the ability of precursor IELs entering the IEC layer to possess a granular cytoplasmic structure and to express CD8αα molecules with no relation to presence or absence of a thymus, TCR expression, or intestinal flora.

It is well known that antigen-specific αβ-IELs have a protective role against infection by pathogenic microorganisms, but ligands of cytotoxicity expressed by αβ-IELs and γδ-IELs from specific pathogen-free mice and γδ-IELs from germ-free mice are still not clear. Do these cytotoxic IELs present in the harsh microenvironments at the front line of intestinal mucosa correctly identify target cells by TCR? Even without very strict specificity, are IECs that have been damaged by stress, viral infections, bacterial infections, or transformed IECs rapidly detected and are these dubious IECs eliminated? Are these cytotoxic IELs indiscriminate predators lurking savagely in the jungle of the IEC layer (Fig. 8)? What T cells are these IELs anyway? In any event, elucidation of these conditions is very important to clarify the development and physiological function of IELs.

Conclusion

IELs are known as peripheral T cells with marked specificity and a very large population size, but their development and physiological function remain a mystery. Findings obtained through research over the past 30 years are very important. We view these diverse experimental observations as many tips of an iceberg that must firmly interconnect with its hidden part. Understanding the immunobiology of IELs must begin in the context of intestinal flora, which outnumber the total number of cells in our body and which have evolved with us in a commensal or symbiotic state. Elucidation of the characteristics of immune responses in the intestines, as the frontline defense against pathogens from the outer world, through clarification of the development and physiological function of IELs is essential for manipulation of intestinal immunity for our benefit.

References

1. Guy-Grand D, Griscelli C, Vassalli P. The gut-associated lymphoid system: nature and properties of the large dividing cells. Eur J Immunol 1974;**4**:435–443.
2. Tonegawa S, et al. Diversity, development, ligands, and probable function of γδ T cells. Cold Spring Harb Symp Quant Biol 1989;**54**:31–44.
3. Cerf-Bensussan N, Guy-Grand D, Griscelli C. Intraepithelial lymphocytes of human gut: isolation, characterization and study of natural killer activity. Gut 1985;**26**:81–88.
4. Klein JR. Ontogeny of the $Thy\text{-}1^-$, $Lyt\text{-}2^+$ murine intestinal intraepithelial lymphocyte. Characterization of unique population of thymus-independent cytotoxic effector cells in the intestinal mucosa. J Exp Med 1986;**164**:309–314.
5. Dillon SB, MacDonald TT. Functional characterization of Con A-responsive mouse small intestinal intraepithelial lymphocytes. Immunology 1986;**59**:389–396.
6. Goodman T, Lefrancois L. Expression of the γ-δ T-cell receptor on intestinal $CD8^+$ intraepithelial lymphocytes. Nature 1988;**333**:855–858.
7. Klein JR. Thymus-independent development of gut T cells. Chem Immunol 1998;**71**:88–102.
8. Lefrancois L, Puddington L. Basic aspects of intraepithelial lymphocyte immunobiology. In: Ogra PL, Mestecky J, Lamm ME, Strober W, Bienenstock L, McGhee JR, eds. Mucosal Immunology. San Diego: Academic Press, 1999:413–428.
9. Kronenberg M, Cheroutre H. Development, function, and specificity of intestinal intraepithelial lymphocytes. In: Mestecky J, Lamm ME, Strober W, Bienenstock J, McGhee JR, Mayer L, eds. Mucosal Immunology. San Diego: Academic Press, 2005:565–581.
10. Hayday A, Theodoridis E, Ramsburg E, Shires J. Intraepithelial lymphocytes: exploring the third way in immunology. Nat Immunol 2001;**2**:997–1003.
11. Bandeira A, et al. Extrathymic origin of intestinal intraepithelial lymphocytes bearing T-cell antigen receptor γδ. Proc Natl Acad Sci USA 1991;**88**:43–47.
12. Nonaka S, et al. Intestinal γδ T cells develop in mice lacking thymus, all lymph nodes, Peyer's patches, and isolated lymphoid follicles. J Immunol 2005;**174**:1906–1912.
13. Fichtelius KE. The gut epithelium – a first level lymphoid organ? Exp Cell Res 1968;**49**:87–104.
14. Matsunaga T. Did the first adaptive immunity evolve in the gut of ancient jawed fish? Cytogenet Cell Genet 1998;**80**:138–141.
15. Du Pasquier L, Flajnik M. Origin and evolution of the vertebrate immune system. In: Paul W, ed. Fundamental Immunology. Philadelphia: Lippincott-Raven Publisher, 1999:605–650.
16. Griebel PJ, Hein WR. Expanding the role of Peyer's patches in B-cell ontogeny. Immunol Today 1996;**17**:30–39.

17. Davies M, Parrott D. The early appearance of specific cytotoxic T cells in murine gut mucosa. Clin Exp Immunol 1980;**42**:273–279.
18. Ernst PB, Clark DA, Rosenthal KL, Befus AD, Bienenstock J. Detection and characterization of cytotoxic T lymphocyte precursors in the murine intestinal intraepithelial leukocyte populations. J Immunol 1986;**136**: 2121–2126.
19. Viney J, Kilshaw P, MacDonald T. Cytotoxic α/β^+ and γ/δ^+ T cells in murine intestinal epithelium. Eur J Immunol 1990;**20**: 1623–1626.
20. Correa I, Bix M, Liao N, Zijlstra M, Jaenisch R, Raulet D. Most γδ T cells develop normally in β_2-microglobulin-deficient mice. Proc Natl Acad Sci USA 1992;**89**:653–657.
21. Neuhaus O, Emoto M, Blum C, Yamamoto S, Kaufmann S. Control of thymus-independent intestinal intraepithelial lymphocytes by β_2-microglobulin. Eur J Immunol 1995;**25**:2332–2339.
22. Pennington DJ, et al. The inter-relatedness and interdependence of mouse T cell receptor $\gamma\delta^+$ and $\alpha\beta^+$ cells. Nat Immunol 2003;**4**:991–998.
23. Fujiura Y, et al. Development of $CD8\alpha\alpha^+$ intestinal intraepithelial T cells in β_2-microglobulin- and/or TAP1-deficient mice. J Immunol 1996;**156**:2710–2715.
24. Leishman AL, et al. T cell responses modulated through interaction between $CD8\alpha\alpha$ and the nonclassical MHC molecules, TL. Science 2001;**294**:1936–1939.
25. Leishman AJ, et al. Precursor of functional MHC class I- or class II-restricted $CD8\alpha\alpha^+$ T cells are positively selected in the thymus by agonist self-peptides. Immunity 2002;**16**:355–364.
26. Lefrancois L, Puddington L. Extrathymic intestinal T-cell development: virtual reality? Immunol Today 1995;**16**:16–21.
27. Rocha B, Guy-Grand D, Vassalli P. Extrathymic T cell differentiation. Curr Opin Immunol 1995;**7**:235–242.
28. Poussier P, Julius M. Speculation on the lineage relationship among $CD4^-8^+$ gut-derived T cells and their role(s). Semin Immunol 1999;**11**:293–303.
29. Guy-Grand D, Vassalli P. Gut intraepithelial lymphocyte development. Curr Opin Immunol 2002;**14**:255–259.
30. Ishikawa H, Kanamori Y, Hamada H, Kiyono H. Development and function of organized gut associated lymphoid tissues. In: Mestecky J, Lamm ME, Strober W, Bienenstock J, McGhee JR, Mayer L, eds. Mucosal Immunology. San Diego: Academic Press, 2005:285–405.
31. Kuwata N, Igarashi H, Ohmura T, Aizawa S, Sakaguchi N. Absence of expression of RAG1 in peritoneal B-1 cells detected by knocking into RAG1 locus with green fluorescent protein gene. J Immunol 1999;**163**:6355–6359.
32. Fujimoto M, et al. Complementary role for CD19 and Bruton's tyrosine kinase in B lymphocyte signal transduction. J Immunol 2002;**168**:5465–5476.
33. Ota Y, et al. Extrathymic origin of Vγ1/Vδ6 T cells in the skin. Eur J Immunol 1992;**22**:595–598.
34. Matis LA, Cron R, Bluestone JA. Major histocompatibility complex-linked specificity of γδ receptor-bearing T lymphocytes. Nature 1987;**330**:262–264.
35. Yoshikai Y, et al. Functional T cell receptor δ chain gene messages in athymic nude mice. Eur J Immunol 1988;**18**:1039–1043.
36. Kanamori Y, et al. Identification of novel lymphoid tissues in murine intestinal mucosa where clusters of $c\text{-}kit^+IL\text{-}7R^+$ $Thy1^+$ lympho-hemopoietic progenitors develop. J Exp Med 1996;**184**:1449–1459.
37. Hamada H, et al. Identification of multiple isolated lymphoid follicles on the antimesenteric wall of the mouse small intestine. J Immunol 2002;**168**:57–64.
38. Suzuki K, et al. Gut cryptopatches: direct evidence of extrathymic anatomical sites for intestinal T lymphopoiesis. Immunity 2000;**13**:691–702.
39. Saito H, et al. Generation of intestinal T cells from progenitors residing in gut cryptopatches. Science 1998;**280**:275–278.
40. Oida T, et al. Role of gut cryptopatches in early extrathymic maturation of intestinal intraepithelial T cells. J Immunol 2000;**164**:3616–3626.
41. Podd BS, et al. T cells in cryptopatch aggregates share TCR γ variable region junctional sequences with γδ T cells in the small intestinal epithelium of mice. J Immunol 2006;**176**:6532–6542.
42. Lambolez F, et al. Characterization of T cell differentiation in the murine gut. J Exp Med 2002;**195**:437–449.
43. Guy-Grand D, et al. Exrathymic T cell lymphopoiesis: ontogeny and contribution to gut intraepithelial lymphocytes in athymic and euthymic mice. J Exp Med 2003;**197**: 333–341.
44. Lin T, Matsuzaki G, Kenai H, Nomoto K. Progenies of fetal thymocytes are the major source of $CD4^-CD8\alpha\alpha^+$ intestinal intraepithelial lymphocytes early in ontogeny. Eur J Immunol 1994;**24**: 1785–1791.
45. Wang J, Klein JR. Thymus-neuroendocrine interactions in extrathymic T cell development. Science 1994;**265**:1860–1862.
46. Wang J, Whetsell M, Klein JR. Local hormone networks and intestinal T cell homeostasis. Science 1997;**275**:1937–1939.
47. Dejbakhsh-Jones S, Jerabek L, Weissman IL, Strober S. Extrathymic maturation of αβ T cells from hemopoietic stem cells. J Exp Med 1999;**155**:3338–3344.
48. Simizu T, et al. The majority of lymphocytes in the bone marrow, thymus and extrathymic T cells in the liver are generated in situ from their own preexisting precursors. Microbiol Immunol 1999;**43**:595–608.
49. Arcangeli M-L, et al. Extrathymic hemopoietic progenitors committed to T cell differentiation in the adult mouse. J Immunol 2005;**174**:1980–1988.
50. Eberl G, Littman DR. Thymic origin of intestinal αβ T cells revealed by fate mapping of $ROR\gamma t^+$ cells. Science 2004;**305**:248–251.
51. Maki K, Sunaga S, Ikuta K. The V-J recombination of T cell receptor-γ genes is blocked in interleukin-7 receptor-deficient mice. J Exp Med 1996;**184**:2423–2427.
52. Taylor RT, Lugering A, Newell AN, Williams IR. Intestinal cryptopatch formation in mice requires lymphotoxin α and the lymphotoxin β receptor. J Immunol 2004;**173**: 7183–7189.
53. Deusch K, Luling F, Reich K, Classen M, Wagner H, Pfeffer K. A major fraction of human intraepithelial lymphocytes simultaneously expresses the γ/δ T cell receptor, the CD8 accessory molecule and preferentially uses the Vδ1 gene segment. Eur J Immunol 1991;**21**:1053–1059.
54. Lundqvist C, Baranov V, Hammarstrom S, Athlin L, Hammarstrom ML. Intra-epithelial lymphocytes. Evidence for regional specialization and extrathymic T cell maturation in the human gut epithelium. Int Immunol 1995;**7**:1473–1487.
55. Jarry A, Cerf-Bensussan N, Brousse N, Selz F, Guy-Grand D. Subsets of $CD3^+$ (T cell receptor α/β or γ/δ) and $CD3^-$ lymphocytes isolated from normal human gut epithelium display phenotypical features different from their counterparts in peripheral blood. Eur J Immunol 1990;**20**:1097–1103.
56. Latthe M, Terry L, MacDonald TT. High frequency of $CD8\alpha\alpha$ homodimer-bearing T cells in human fetal intestine. Eur J Immunol 1994;**24**:1703–1705.
57. Lynch S, Kelleher D, McManus R, O'Farrelly C. RAG1 and RAG2 expression in human intestinal epithelium: evidence of extrathymic T cell differentiation. Eur J Immunol 1995;**25**:1143–1147.
58. Koningsberger JC, et al. TCR expression in human fetal intestine and identification of an early T cell receptor β-chain transcript. J Immunol 1997;**159**:1775–1782.
59. Howie D, et al. Extrathymic T cell differentiation in the human intestine early in life. J Immunol 1998;**161**:5862–5872.
60. Ramanathan S, Marandi L, Poussier P. Evidence for the extrathymic origin of intestinal $TCR\gamma\delta^+$ T cells in normal rats and for an impairment of this differentiation pathway in BB rats. J Immunol 2002;**168**: 2182–2187.

61. Hitotsumatsu O, et al. Identification and characterization of novel gut-associated lymphoid tissues in rat small intestine. J Gastroenterol 2005;**40**:956–963.
62. Mayrhofer G, Moghaddami M, Murphy C. Lymphocyte-filled villi (LFV): non-classical organized lymphoid tissues in the mucosa of the small intestine. Mucosal Immunol Update 1999;**7**:9–13.
63. Jemeson J, et al. A role for skin γδ T cells in wound repair. Science 2002;**296**:747–749.
64. Jemeson JM, Cauvi G, Deborah A, Witherden DA, Havran WL. A keratinocyte-responsive γδ TCR is necessary for dendritic epidermal T cell activation by damaged keratinocytes and maintenance in the epidermis. J Immunol 2004;**172**:3573–3579.
65. Ferguson A. Intraepithelial lymphocytes of the small intestine. Gut 1977;**18**:921–937.
66. Mysorekar IU, Lorenz RG, Gordon JI. A gnotobiotic transgenic mouse model for studying interactions between small intestinal enterocytes and intraepithelial lymphocytes. J Biol Chem 2002;**277**:37811–37819.
67. Rocha B, Vassalli P, Guy-Grand D. The Vβ repertoire of mouse gut homodimeric α $CD8^+$ intraepithelial T cell receptor α/β^+ lymphocytes reveals a major extrathymic pathway of T cell differentiation. J Exp Med 1991;**173**:483–486.
68. Page ST, et al. Intestinal intraepithelial lymphocytes include precursors committed to the T cell receptor αβ lineage. Proc Natl Acad Sci USA 1998;**95**:9459–9464.
69. Poussier P, Edouard P, Lee C, Binnie M, Julius M. Thymus-independent development and negative selection of T cells expressing T cell receptor α/β in the intestinal epithelium: evidence for distinct circulation patterns of gut- and thymus-derived T lymphocytes. J Exp Med 1992;**176**:187–199.
70. Suzuki S, et al. Low level of mixing of partner cells seen in extrathymic T cells in the liver and intestine of parabiotic mice: its biological implication. Eur J Immunol 1998;**28**:3719–3729.
71. Stappenbeck TS, Wong MH, Saam JR, Mysorekar IU, Gordon JI. Notes from some crypt watchers: regulation of renewal in the mouse intestinal epithelium. Curr Opin Cell Biol 1998;**10**:702–709.
72. Penney L, Kilshaw PJ, MacDonald TT. Regional variation in the proliferative rate and lifespan of αβ TCR^+ and γδ TCR^+ intraepithelial lymphocytes in the murine small intestine. Immunology 1995;**86**:212–218.
73. Balk SP, et al. Oligoclonal expansion and CD1 recognition by human intestinal intraepithelial lymphocytes. Science 1991;**253**:1411–1415.
74. Van Kerckhove, et al. Oligoclonality of human intestinal intraepithelial T cells. J Exp Med 1992;**175**:57–63.
75. Blumberg RS, Yockey CE, Grass GG, Ebert EC, Balk SP. Human intestinal intraepithelial lymphocytes are derived from a limited number of T cell clones that utilize multiple Vβ T cell receptor genes. J Immunol 1993;**150**:5144–5153.
76. Regnault A, Cumano A, Vassalli P, Guy-Grand D, Kourilsky P. Oligoclonal repertoire of the CD8αα and the CD8αβ TCR-α/β murine intestinal intraepithelial T lymphocytes: evidence for the random emergence of T cells. J Exp Med 1994;**180**:1345–1358.
77. Regnault A, et al. The expansion and selection of T cell receptor αβ intestinal intraepithelial clones. Eur J Immunol 1996;**26**:914–921.
78. Guy-Grand D, Malassis-Seris M, Briottet C, Vassalli P. Cytotoxic differentiation of mouse gut thymodependent and independent intraepithelial T lymphocytes is induced locally. Correlation between functional assays, presence of perforin and granzyme transcripts, and cytoplasmic granules. J Exp Med 1991;**173**:1549–1552.
79. Goodman T, Lefrancois L. Intraepithelial lymphocytes. Anatomical site, not T cell receptor form, dictates phenotype and function. J Exp Med 1989;**170**:1569–1581.
80. Ishikawa H, Li Y, Abeliovich A, Yamamoto S, Kaufmann HE, Tonegawa S. Cytotoxic and interferon γ-producing activities of γδ T cells in the mouse intestinal epithelium are strain dependent. Proc Natl Acad Sci USA 1993;**90**:8204–8208.
81. Kawaguchi M, et al. Cytolytic activity of intestinal intraepithelial lymphocytes in germ-free mice is strain dependent and determined by T cells expressing γδ T-cell antigen receptors. Proc Natl Acad Sci USA 1993;**90**:8591–8594.
82. Croitoru K, et al. Presence of intestinal lymphocytes in mice with severe combined immunodeficiency disease. Eur J Immunol 1990;**20**:645–651.
83. Takahashi-Iwanaga H, Iwanaga T, Sakamoto Y, Fujita T. Ultrastructural and time-lapse observation of intraepithelial lymphocytes in the small intestine of the guinea pig: their possible role in the removal of effete enterocytes. Cell Tissue Res 1995;**280**:491–497.

AJP - Lung Cellular and Molecular Physiology publishes original research covering the broad scope of molecular, cellular, and integrative aspects of normal and abnormal function of cells and components of the respiratory system. It is published 12 times a year (monthly) by the American Physiological Society, 9650 Rockville Pike, Bethesda MD 20814-3991. Copyright © 2005 by the American Physiological Society. ISSN: 1040-0605, ESSN: 1522-1504. Visit our website at http://www.the-aps.org/.

Am J Physiol Lung Cell Mol Physiol 290: L1059–L1068, 2006.
First published December 30, 2005; doi:10.1152/ajplung.00365.2005.

Various adhesion molecules impair microvascular leukocyte kinetics in ventilator-induced lung injury

Naoki Miyao,[1] Yukio Suzuki,[3] Kei Takeshita,[3] Hiroyasu Kudo,[1] Makoto Ishii,[1] Rika Hiraoka,[1] Kazumi Nishio,[1] Takuya Tamatani,[4] Shinji Sakamoto,[4] Makoto Suematsu,[2] Harukuni Tsumura,[5] Akitoshi Ishizaka,[1] and Kazuhiro Yamaguchi[1]

Departments of [1]Medicine and [2]Biochemistry, School of Medicine, Keio University, Tokyo; [3]Department of Medicine, Kitasato Institute Hospital, Tokyo; [4]Pharmaceutical Frontier Research Laboratories, JT Incorporated, Yokohama; and [5]Biochemical Department, Sankei Corporation, Tokyo, Japan

Submitted 22 August 2005; accepted in final form 28 December 2005

Miyao, Naoki, Yukio Suzuki, Kei Takeshita, Hiroyasu Kudo, Makoto Ishii, Rika Hiraoka, Kazumi Nishio, Takuya Tamatani, Shinji Sakamoto, Makoto Suematsu, Harukuni Tsumura, Akitoshi Ishizaka, and Kazuhiro Yamaguchi. Various adhesion molecules impair microvascular leukocyte kinetics in ventilator-induced lung injury. *Am J Physiol Lung Cell Mol Physiol* 290: L1059–L1068, 2006. First published December 30, 2005; doi:10.1152/ajplung.00365.2005.—Although the endothelial expression of various adhesion molecules substantially differs between pulmonary microvessels, their importance for neutrophil and lymphocyte sequestration in ventilator-induced lung injury (VILI) has not been systematically analyzed. We investigated the kinetics of polymorphonuclear cells (PMN) and mononuclear cells (MN) in the acinar microcirculation of the isolated rat lung with VILI by real-time confocal laser fluorescence microscopy, with or without inhibition of ICAM-1, VCAM-1, or P-selectin by monoclonal antibodies (MAb). Adhesion molecules in each microvessel were estimated by intravital fluorescence microscopy or immunohistochemical staining. In high tidal volume-ventilated lungs, *1*) ICAM-1, VCAM-1, and P-selectin were differently upregulated in venules, arterioles, and capillaries; *2*) venular PMN rolling was improved by inhibition of ICAM-1, VCAM-1, or P-selectin, whereas arteriolar PMN rolling was improved by ICAM-1 or VCAM-1 inhibition; *3*) capillary PMN entrapment was ameliorated only by anti-ICAM-1 MAb; and *4*) MN rolling in venules and arterioles and MN entrapment in capillaries were improved by ICAM-1 and VCAM-1 inhibition. In conclusion, the contribution of endothelial adhesion molecules to abnormal leukocyte behavior in VILI-injured microcirculation is microvessel and leukocyte specific. ICAM-1- and VCAM-1-dependent, but P-selectin-independent, arteriolar PMN rolling, which is expected to reflect the initial stage of tissue injury, should be taken as a phenomenon unique to ventilator-associated lung injury.

neutrophil; lymphocyte; rolling; adhesion

MECHANICAL VENTILATION PLAYS a major role as a tool for basic life support, especially for treating patients with acute respiratory distress syndrome. However, many studies have ascertained that sustained artificial ventilation with a tidal volume set to maintain arterial P_{CO_2} (Pa_{CO_2}) at a normal level leads to worsening of lung injury, which has been defined as ventilator-induced lung injury (VILI) (6). VILI has been shown to be caused by the augmented mechanical stress related to overdistension of lung units and, probably, cyclical airway closure and reopening, resulting in promotion of a neutrophil-evoked inflammatory response concomitant with significant neutrophil infiltration into the lung tissue and increased levels of various inflammatory cytokines in the bronchoalveolar lavage (BAL) fluid (BALF) (15, 26, 28, 31).

The accumulation of neutrophils in the lung tissue is initially mediated through increased adhesion of neutrophils to endothelial cells of the inflamed pulmonary microvasculature, and this process requires the upregulation of various adhesion molecules expressed on the surface of pulmonary microvessel endothelial cells as well as circulating neutrophils (18, 22). Despite the importance of augmented expression of adhesion molecules for initiating neutrophil-evoked lung injury, there has been little study shedding light on this issue in lung models of VILI, except that reported by Yiming et al. (37). These authors demonstrate that P-selectin expression on endothelial cells of the pulmonary vasculature was enhanced at an early stage after commencing artificial ventilation with a high tidal volume, followed by neutrophil accumulation. Unfortunately, however, they did not analyze other important adhesion molecules mediating neutrophil adhesion to pulmonary endothelial cells, such as ICAM-1 and VCAM-1. Furthermore, the relative contribution of each hierarchy of microvessels, including arterioles, venules, and capillaries, to neutrophil sequestration to the pulmonary microcirculation has never been examined in a VILI model, although this approach is essential for deepening our understanding of the early pathogenesis of VILI.

In addition to neutrophil infiltration in the lung tissue, lymphocyte accumulation and activation may occur at sites of inflammation in VILI. However, there has been no reliable study analyzing the contribution of lymphocytes to the initiation and/or aggravation of VILI. Lymphocytes may have a number of functions, including immune response, release of various cytokines, and cytotoxicity (36), all of which are expected to play a pivotal role in the development and pathogenesis of VILI. Although the recruitment of lymphocytes to inflammatory sites in systemic organs and tissues has been shown to be mediated in part through an adhesive mechanism involving ICAM-1- and/or VCAM-1-dependent pathways (2, 34), the issue of whether the same holds true for lymphocyte recruitment to the microcirculation of the diseased lung has not been extensively addressed.

To elucidate the adhesive mechanism mediating the accumulation of neutrophils and lymphocytes in arterioles, venules, or capillaries in lungs injured by sustained artificial mechanical

Address for reprint requests and other correspondence: Y. Suzuki, Dept. of Medicine, Kitasato Institute Hospital, 5-9-1, Shirokane, Minato-ku, Tokyo 108-8642, Japan (e-mail: suzuki-yk@kitasato.or.jp).

The costs of publication of this article were defrayed in part by the payment of page charges. The article must therefore be hereby marked "*advertisement*" in accordance with 18 U.S.C. Section 1734 solely to indicate this fact.

ventilation, we analyzed the following issues: *1*) differential expression of various classes of adhesion molecules, including ICAM-1, VCAM-1, and P-selection, along arteriolar, venular, and capillary walls in a rat model of VILI; *2*) measurements of the dynamic behavior of polymorphonuclear cells (PMN: mainly composed of neutrophils) within arterioles, venules, and capillaries in the lung isolated from an animal exposed to prolonged ventilation by means of recently developed real-time confocal laser fluorescence microscopy in the presence or absence of MAb to each endothelial adhesion molecule; and *3*) confocal microscopic measurements of the dynamic behavior of mononuclear cells (MN: mainly consisting of lymphocytes) in each microvessel of the isolated lung with VILI, with and without MAb, to the respective adhesion molecules.

METHODS

Animals with VILI, fluorescein-labeled leukocytes, and isolated perfused lungs. All animals received care according to the "Principles of Laboratory Animal Care" formulated by the National Society for Medical Research. Specific pathogen-free Sprague-Dawley male rats, 8 wk of age, weighing 250–300 g, were anesthetized by intraperitoneal injection of 50 mg/kg pentobarbital followed by intermittent injection of 10 mg/kg pentobarbital every hour (n = 41). No muscle relaxant was used for anesthetization. To induce ventilator-associated lung injury, anesthetized Sprague-Dawley rats were artificially ventilated with a volume-controlled ventilator (KN-55 Natsume Seisakusho, Tokyo, Japan) with room air at a constant tidal volume of 15 ml/kg and respiratory rate of 35 breaths/min, with no positive end-expiratory pressure (PEEP) for 6 h (n = 18). On the other hand, animals ventilated with room air at a constant tidal volume of 7.5 ml/kg and respiratory rate of 70 breaths/min without PEEP for 6 h were assigned to the low tidal group (n = 10). These animals were divided into several groups depending on the leukocyte type observed (PMN or MN) and the MAb used to inhibit adhesion molecules (ICAM-1, VCAM-1, and P-selectin) expressed on the endothelial surface of pulmonary microvessels (see *Experimental protocols*). Spontaneously ventilated animals with room air without anesthesia were assigned to the control group (n = 13). Accumulation of PMN and MN in the alveolar septa and BALF was examined in the control, low tidal, and high tidal groups. The density of leukocytes in the septa was expressed as the number per single alveolus.

Preparation of fluorescein-labeled PMN and MN. We aspirated whole blood from the left ventricle of normal donor rats, in which 28 ± 9% of leukocytes were PMN and the remainder were MN (lymphocytes: 72 ± 9%). We isolated PMN and MN from whole blood aspirated from donor rats by applying a classic Ficoll density gradient procedure adapted for either rat PMN (specific gravity: 1.112) or MN (specific gravity: 1.090) (20). Both cell layers were labeled with carboxyfluorescein diacetate succinimidyl ester (CFDASE). This fluorescence precursor yields carboxyfluorescein succinimidyl ester (CFSE) in leukocytes but not in erythrocytes (27). After 30-min incubation of each leukocyte layer with CFDASE in vitro, the final solution was added to the perfusion reservoir connected to the isolated perfused lung system (see below). Preliminary experiments confirmed that the layer of PMN separated by the Ficoll method was mostly composed of neutrophils (96 ± 0.8%). In the layer of MN obtained by qualitatively the same method as applied for PMN, most of the blood cells were found to be lymphocytes (99 ± 0.5%). Leukocytes (PMN and MN) and platelets stained with CFSE were easily distinguishable during microscopic observation because of their distinctive difference in size.

Preparation of isolated perfused lungs. The animals with 6-h artificial ventilation were not anesthetized again, but the control animals were anesthetized with pentobarbital (50 mg/kg, intraperitoneally). These animals were artificially ventilated with room air for only the short time necessary to prepare the isolated perfused lung system. After median sternotomy was performed, animals were killed by exsanguination, and cannulas were inserted into the pulmonary artery and left atrium. Both cannulas were secured with ligatures. A ligature was placed around the aorta to prevent loss of perfusate into the systemic circulation. Isolated lungs prepared from the control, low tidal, and high tidal groups were fixed on a microscope stage in the supine position and perfused at a constant flow rate of 10 ml/min with physiological solution containing a small amount of whole blood ~10 min after exsanguination. Modified Krebs-Henseleit solution was used as the perfusate, and 3% bovine serum albumin was added to maintain isoosmotic pressure. Perfusate hematocrit was adjusted to 3.2 ± 0.8% by the addition of fresh blood obtained from donor rats, which were pretreated with 5 mg/kg heparin. Because the total volume of perfusate was adjusted to 100 ml, heparin concentration in the circulation system was ~6.5 μg/ml. To avoid movement caused by artificial ventilation, the trachea was ligated at the end-inspiratory point, and gas exchange was maintained with an extracorporeal membrane oxygenator (ECMO, Merasilox-S; Senko, Tokyo, Japan). A gas mixture containing 21% O_2 and 5% CO_2 in N_2 was used as the gas flowing into the ECMO, resulting in perfusate Po_2, Pco_2, and pH of 142 ± 6 Torr, 37 ± 2 Torr, and 7.41 ± 0.03, respectively. A warmed and humidified gas mixture containing the same composition of gases as those used for the ECMO was continuously supplied to the lung surface to maintain a temperature of 37 ± 0.2°C and to avoid desiccation of the lung surface. Pulmonary arterial pressure was continuously monitored by force displacement of a pressure transducer (TP-400T; Nihon Kohden, Tokyo, Japan).

Experimental protocols. To investigate the effects of various adhesion molecules on the microcirculatory behavior of leukocytes in the early stage of VILI, we designed six experiments for both CFSE-stained PMN and CFSE-stained MN: *1*) Control group (PMN n = 6, MN n = 7): animals breathed spontaneously without a ventilator and anesthesia. *2*) Low tidal group (PMN n = 5, MN n = 5): animals were ventilated with a tidal volume of 7.5 ml/kg for 6 h. *3*) High tidal group (PMN n = 9, MN n = 9): animals were ventilated with a tidal volume of 15 ml/kg for 6 h. *4*) ICAM-1 group (PMN n = 6, MN n = 8): MAb against rat ICAM-1 (1A29; donated by Dr. Miyasaka, Osaka University Medical School, Osaka, Japan) was administered to isolated perfused lungs prepared from animals with VILI. Perfusate concentration of 1A29 was maintained at 20 μg/ml. After 10-min perfusion with 1A29, the microcirculatory behavior of PMN or MN was investigated. The efficiency of 1A29 in blocking rat ICAM-1 was extensively discussed by Tamatani and Miyasaka (29). *5*) VCAM-1 group (PMN n = 5, MN n = 7): MAb against rat VCAM-1 (MR106; donated by Dr. Yagita, Juntendo University, School of Medicine) was administered at a final concentration of 20 μg/ml into perfused lungs prepared from the animals with high tidal volume ventilation. Ten minutes after the addition of MR106, PMN or MN kinetics was observed. *6*) P-selectin group (PMN n = 6, MN n = 5): MAb against rat P-selectin (s789G) was administered at a final concentration of 20 μg/ml into perfused lungs prepared from the animals with high tidal volume ventilation. Ten minutes later, PMN or MN kinetics was examined. The specificity of s789G in inhibiting rat P-selectin is described in detail elsewhere (11).

Observation of microvascular cell kinetics by confocal fluorescence microscopy. We used a real-time confocal laser scanning fluorescence optical microscope (CSU10; Yokokawa, Tokyo, Japan) incorporating a high-speed video analysis system (35). The reflected light or fluorescent emission from the specimen was imaged onto a high-sensitivity charge-coupled device (CCD) camera with an image intensifier (VSG; Kodak, San Diego, CA). By incorporating an excitation wave length of 488 nm emitted from a low-power air-cooled argon laser (532-BSA04; Omnichrome, Cino, CA), the present confocal system allowed us to obtain apparently instantaneous images at 1,000 frames/s. The final magnifying power of our system reached

×484 with a ×20 objective. We obtained confocal images of microvessels on the plane that was in focus at 5–25 μm distance from the surface of the left upper lung. We registered confocal images at a rate of 125 frames/s with a high-speed digital video analysis system (1000 Processor; Kodak, Tokyo, Japan) connected to the image-intensified CCD camera. All images were stored on the hard disk of a personal computer.

To examine the erythrocyte velocity (Vr) in the same microvessel used for assessment of PMN or MN behavior, erythrocytes were stained with fluorescein isothiocyanate (FITC; Sigma, St. Louis, MO). Fresh rat blood was centrifuged at 1,000 rpm for 5 min, and the buffy coat was discarded. The packed erythrocyte solution was diluted with PBS, and FITC was added to give a final concentration of 0.1 mg/ml. This solution was added to the reservoir after PMN or MN kinetics had been measured, and then erythrocyte kinetics was determined, as well.

To examine the architecture of microvessels in which leukocyte and erythrocyte behavior had been analyzed, 200 μl of 5% FITC-dextran with a molecular weight of 145,000 (Sigma) were added to the reservoir. The microvessel from which fluorescein-labeled blood cells entered the capillary network was defined as the arteriole, whereas the microvessel into which blood cells flowed from the capillary network was taken to be the venule.

Quantitative analysis of cell kinetics in arterioles, venules, and capillaries. The highest value of Vr was assumed to be equal to the centerline velocity (Vmax) in a given arteriole or venule. Vmax was used to estimate mean fluid flow (Vmean) in each microvessel, where Vmean = Vmax/1.6 (8). Wall shear rate (γ) was estimated from the equation: $\gamma = 8$ (Vmean/D), where D represents vessel diameter (23). An adherent leukocyte in an arteriole or venule was defined as a cell that was firmly attached to the vascular endothelium and did not move during the observation period. Rolling leukocytes in arterioles and venules were defined as cells transiently interacting with the vascular endothelium and thus traveling much more slowly than centerline erythrocytes. We identified these cells by applying the velocity criterion proposed by Gaehtgens and colleagues (8), who calculated the critical velocity (Vcrit) of a freely flowing cell traveling close to, but not adhering to, the microvascular wall. Vcrit is defined as Vmean$(2-\epsilon)\epsilon$, where ϵ is the ratio of the leukocyte diameter to the microvessel diameter. Any cell flowing at a velocity below Vcrit was assumed to be slowed by the interaction with the vascular endothelium and defined as a rolling cell.

To quantify the cell transit in capillaries, we classified the observed leukocytes into two categories: *1*) cells moving smoothly without interruption and 2) impeded cells stopping for >20 ms within a capillary segment, thus including the cells with transient entrapment and those with sustained arrest in capillaries during the observation period.

Intravital determination of ICAM-1, VCAM-1, and P-selectin expression along microvessel walls. We examined the expression of ICAM-1, VCAM-1, and P-selectin along microvessel walls by applying the intravital fluorescence microscopic method ($n = 3$ for each). This method allows reliable separation of arterioles from venules in association with quantitative determination of each adhesion molecule expressed along microvessel walls. In brief, 4 μg/g body wt of 1A29 (MAb against ICAM-1), MR106 (MAb against VCAM-1), or s789G (MAb against P-selectin) were injected into the pulmonary artery via the perfusion catheter. Ten minutes later, 0.5 ml of FITC-labeled anti-mouse IgG antibody (Sigma), the secondary antibody to each MAb, was injected into an isolated perfused lung. Subsequently, flow was stopped for 15 min to allow conjugation of a given adhesion molecule on the vascular endothelium, its MAb, and FITC-IgG antibody. The final complex of the adhesion molecule bound to its MAb and FITC-IgG antibody was examined under a confocal scanning fluorescence microscope and displayed on a high-sensitivity CCD camera (TEC-470; Optronics, Goleta, CA). As the MAb used in the present study consisted of mouse IgG, IgG raised in mice (4 μg/g body wt, Sigma) and FITC-labeled anti-mouse IgG antibody were used as negative controls. Arterioles, venules, and capillaries were distinguished by administering both FITC-dextran and FITC-labeled erythrocytes at the end of each measurement. We measured the complex-elicited fluorescence intensity along microvessel walls by processing a confocal image with a digital image-analyzing system (Quadra 840AV/Image 1.58; Apple, Cupertino, CA).

Determination of ICAM-1, VCAM-1, and P-selectin expression by immunohistochemical staining. The lungs with high tidal volume ventilation were fixed by administration of periodate-lysine-paraformaldehyde solution through the trachea, embedded in optimum cutting temperature compound (Miles, Elkhart, IN), and then frozen in dry ice and acetone ($n = 5$). Frozen sections 4 μm in thickness were cut on a cryostat and fixed on slides in cold acetone for 10 min and overnight at −20°C. These sections were washed with PBS, and nonspecific staining was inhibited by incubation with 10% normal pig serum (COSMO BIO, Tokyo, Japan) in PBS for 20 min at room temperature. The sections were then incubated with anti-ICAM-1 (M-19; Santa Cruz Biotechnology, Santa Cruz, CA), anti-VCAM-1 (C-19, Santa Cruz), or anti-P-selectin antibody (C-20, Santa Cruz) diluted 10-fold with PBS, for 1 h at room temperature. After these sections were rinsed with PBS, they were incubated with a 100-fold dilution of secondary antibody (anti-goat IgG-horseradish peroxidase, Santa Cruz) for 1 h at room temperature. After they were rinsed with PBS, they were incubated with 20 mg 3,3′-diaminobenzidine tetrahydrochloride and 20 μl of 30% hydrogen peroxide in 100 ml of PBS for 2 min at room temperature. After washing them in water, we performed counterstaining of nuclei with methyl green. Immunoreactivity for ICAM-1, VCAM-1, or P-selectin in each lung section was determined with a light microscope. In total, 30 sections obtained from each of the upper, middle, and lower lung fields of five different animals were used for immunohistochemical assessment of ICAM-1, VCAM-1, and P-selectin expression in the control, low tidal volume-ventilated and VILI lungs, respectively.

Histological examination and BAL. The lungs harvested from control and low and high tidal volume-ventilated rats were inflated with formalin at a pressure of 30 cmH_2O for 48 h ($n = 5$ for each). Six sections, cut at identical intervals from the apex to the base of the left lung, were embedded in paraffin and stained with hematoxylin-eosin. In each section, 10 fields were randomly chosen, and leukocytes localized within the alveolar septa in which the capillary network is located were counted at a magnification of ×1,000 with an oil immersion lens. The density of leukocytes in the septa was expressed as the number per single alveolus. The same lung sections were used for estimating leukocyte differential counts, i.e., the distinction between PMN and MN. The histological samples obtained from each animal were evaluated in a double-blinded fashion by two doctors.

BAL was carried out by washing the lung with 3 ml pf phosphate-buffered saline twice. The number of total cells and the differential cell counts were determined on Diff-Quick-stained preparations (Kokusai Shiyaku, Kobe, Japan).

Statistical analysis. The results are presented as means ± SD. Significant differences in the frequency of rolling cells (PMN and MN), their capillary entrapment, and their accumulation in alveolar septa among experimental groups (i.e., Control, Low, High, High+anti-ICAM-Ab, High+VCAM-Ab, and High+P-selectin-Ab groups) were determined by applying one-way analysis of variance (ANOVA) followed by Scheffé's multiple-comparison analysis. The values obtained for arterioles, venules, and capillaries in respective experimental conditions were statistically examined by two-way ANOVA together with Scheffé's analysis for multiple comparisons. A P value <0.05 was taken to be statistically significant.

RESULTS

Basic characteristics of lungs with VILI. The BALF concentrations of LDH and protein in the high tidal group were

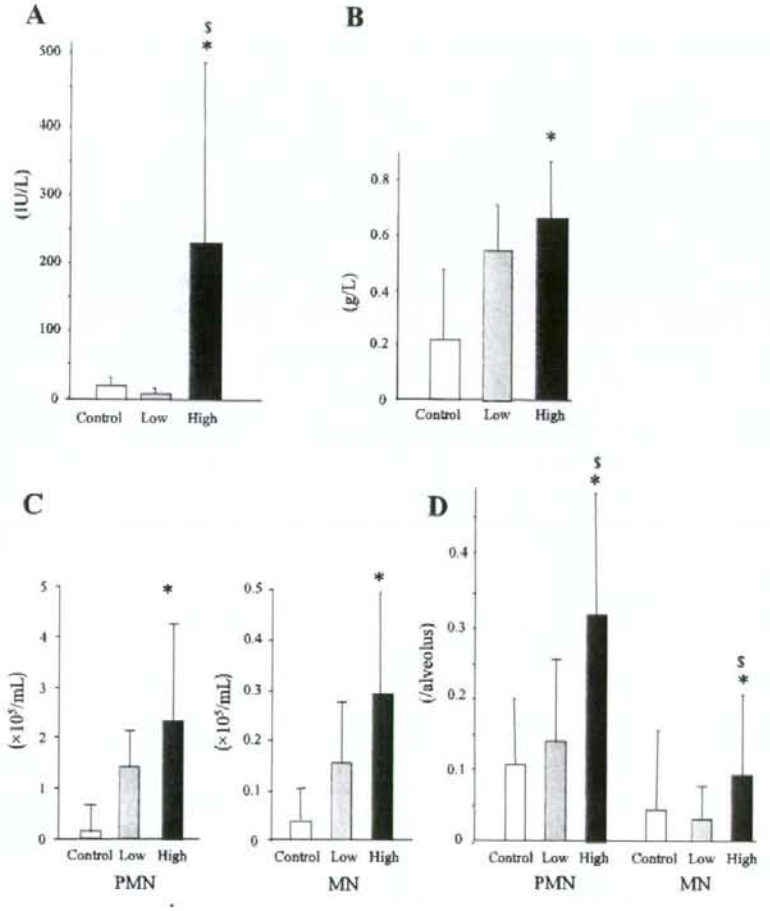

Fig. 1. Biochemical and morphological data observed for control lungs (Control), low tidal volume-ventilated lungs (Low), and high tidal volume-ventilated lungs (High). *A*: LDH concentration in bronchoalveolar lavage fluid (BALF). *B*: protein concentration in BALF. *C*: number of polymorphonuclear cells (PMN) and mononuclear cells (MN) in BALF. *D*: number of PMN and MN within alveolar septa estimated from lung tissue sections stained with hematoxylin-eosin. The density of leukocytes in the septa is expressed as the number per single alveolus. *Significantly different from value in control lungs; $significantly different from value in low tidal volume-ventilated lungs.

markedly higher than those in the control and low tidal groups (Fig. 1, *A* and *B*, respectively). In addition, the numbers of PMN and MN in BALF collected from the high tidal group were much higher than those in the control and low tidal groups (Fig. 1*C*).

The inspiratory peak airway pressure was 8.6 ± 0.7 cmH_2O in the high tidal group and 6.3 ± 0.7 cmH_2O in the low tidal group. Pulmonary arterial pressure was 10.6 ± 1.6 cmH_2O in the high tidal group, 8.6 ± 1.8 cmH_2O in the low tidal group ($P < 0.001$ vs. High), and 8.4 ± 1.7 cmH_2O in the control group ($P < 0.001$ vs. High).

In the histological analysis, the high tidal group showed no serious tissue injury but slightly thickened alveolar walls and significant leukocyte infiltration into perivascular and peribronchiolar regions as well as alveolar spaces. The number of PMN accumulated within the alveolar septa in the high tidal group averaged 0.32 ± 0.19/alveolus, being much higher than that in the control group (0.11 ± 0.09/alveolus) and the low tidal group

Fig. 2. *A–C, H–J, N–P*: immunohistochemical examination of upregulation of various adhesion molecules in lungs with ventilator-induced lung injury using respective MAb against ICAM-1, VCAM-1, and P-selectin. *A*: ICAM-1 in control lung. *B*: ICAM-1 in low tidal volume-ventilated lung. *C*: ICAM-1 in high tidal volume-ventilated lung. *H*: VCAM-1 in control lung. *I*: VCAM-1 in low tidal volume-ventilated lung. *J*: VCAM-1 in high tidal volume-ventilated lung. *N*: P-selectin in control lung. *O*: P-selectin in low tidal volume-ventilated lung. *P*: P-selectin in high tidal volume-ventilated lung. Magnification: ×200. See text for further explanation. *D–G*: intravital examination of ICAM-1 expression examined by fluorescence microscopy. *D* and *E*: expression along venular and capillary walls and arteriolar walls in control lung, respectively. *F* and *G*: expression along venular, capillary, and arteriolar walls in high tidal volume-ventilated lung. See text for details. *K–M*: intravital examination of VCAM-1 expression along microvessel walls. *K*: no significant expression along any microvascular walls in control lung. *L*: expression along arteriolar walls in high tidal volume-ventilated lung. *M*: expression along venular walls and capillaries in high tidal volume-ventilated lung. See text for further details. *Q–S*: intravital examination of P-selection expression along microvessel walls. *Q*: no expression along any microvessel in control lung. *R*: expression along arteriolar walls in high tidal volume-ventilated lung. *S*: expression along venular walls in high tidal volume-ventilated lung. P-selectin expression is not detected in capillary segments. See text for further explanation. A, arteriole; V, venule; C, capillary; Br, bronchus.